



## NRC Publications Archive Archives des publications du CNRC

### **Initial structural models of the A $\beta$ 42 dimer from replica exchange molecular dynamics simulations**

Blinov, Nikolay; Khorvash, Massih; Wishart, David S.; Cashman, Neil R.; Kovalenko, Andriy

This publication could be one of several versions: author's original, accepted manuscript or the publisher's version. / La version de cette publication peut être l'une des suivantes : la version prépublication de l'auteur, la version acceptée du manuscrit ou la version de l'éditeur.

For the publisher's version, please access the DOI link below. / Pour consulter la version de l'éditeur, utilisez le lien DOI ci-dessous.

#### **Publisher's version / Version de l'éditeur:**

<https://doi.org/10.1021/acsomega.7b00805>

*ACS Omega*, 2, 11, pp. 7621-7636, 2017-11-07

#### **NRC Publications Record / Notice d'Archives des publications de CNRC:**

<https://nrc-publications.canada.ca/eng/view/object/?id=f6d6252e-1bbf-45c4-b84a-764106b323d4>

<https://publications-cnrc.canada.ca/fra/voir/objet/?id=f6d6252e-1bbf-45c4-b84a-764106b323d4>

Access and use of this website and the material on it are subject to the Terms and Conditions set forth at

<https://nrc-publications.canada.ca/eng/copyright>

READ THESE TERMS AND CONDITIONS CAREFULLY BEFORE USING THIS WEBSITE.

L'accès à ce site Web et l'utilisation de son contenu sont assujettis aux conditions présentées dans le site

<https://publications-cnrc.canada.ca/fra/droits>

LISEZ CES CONDITIONS ATTENTIVEMENT AVANT D'UTILISER CE SITE WEB.

#### **Questions?** Contact the NRC Publications Archive team at

PublicationsArchive-ArchivesPublications@nrc-cnrc.gc.ca. If you wish to email the authors directly, please see the first page of the publication for their contact information.

**Vous avez des questions?** Nous pouvons vous aider. Pour communiquer directement avec un auteur, consultez la première page de la revue dans laquelle son article a été publié afin de trouver ses coordonnées. Si vous n'arrivez pas à les repérer, communiquez avec nous à PublicationsArchive-ArchivesPublications@nrc-cnrc.gc.ca.



# Initial Structural Models of the A $\beta$ 42 Dimer from Replica Exchange Molecular Dynamics Simulations

Nikolay Blinov,<sup>\*,†,‡,§</sup> Massih Khorvash,<sup>§</sup> David S. Wishart,<sup>||</sup> Neil R. Cashman,<sup>§</sup> and Andriy Kovalenko<sup>‡,†</sup>

<sup>†</sup>Department of Mechanical Engineering, University of Alberta, Edmonton, Alberta T6G 1H9, Canada

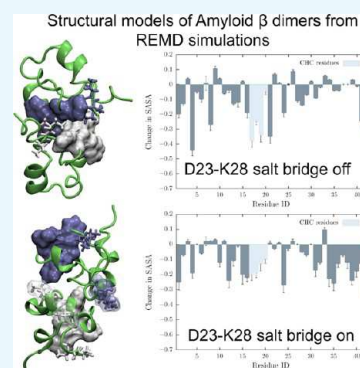
<sup>‡</sup>National Institute for Nanotechnology, National Research Council of Canada, Edmonton, Alberta T6G 2M9, Canada

<sup>§</sup>Department of Medicine, University of British Columbia, Vancouver, British Columbia V6T 2B5, Canada

<sup>||</sup>Departments of Computing Science and Biological Sciences, University of Alberta, Edmonton, Alberta T6G 2E8, Canada

## S Supporting Information

**ABSTRACT:** Experimental characterization of the molecular structure of small amyloid (A) $\beta$  oligomers that are currently considered as toxic agents in Alzheimer's disease is a formidably difficult task due to their transient nature and tendency to aggregate. Such structural information is of importance because it can help in developing diagnostics and an effective therapy for the disease. In this study, molecular simulations and protein–protein docking are employed to explore a possible connection between the structure of A $\beta$  monomers and the properties of the intermonomer interface in the A $\beta$ 42 dimer. A structurally diverse ensemble of conformations of the monomer was sampled in microsecond timescale implicit solvent replica exchange molecular dynamics simulations. Representative structures with different solvent exposure of hydrophobic residues and secondary structure content were selected to build structural models of the dimer. Analysis of these models reveals that formation of an intramonomer salt bridge (SB) between Asp23 and Lys28 residues can prevent the building of a hydrophobic interface between the central hydrophobic clusters (CHCs) of monomers upon dimerization. This structural feature of the A $\beta$ 42 dimer is related to the difference in packing of hydrophobic residues in monomers with the Asp23–Lys28 SB in on and off states, in particular, to a lower propensity to form hydrophobic contacts between the CHC domain and C-terminal residues in monomers with a formed SB. These findings could have important implications for understanding the difference between aggregation pathways of A $\beta$  monomers leading to neurotoxic oligomers or inert fibrillar structures.



## 1. INTRODUCTION

Soluble oligomers composed of amyloid- $\beta$  (A $\beta$ ) peptides are currently considered as neurotoxic agents in Alzheimer's disease (AD).<sup>1–7</sup> A $\beta$  peptides of different length (mostly made of 37–43 residues) originate from proteolytic cleavage of the amyloid precursor protein (APP). Under certain conditions, they can aggregate into amyloid fibrils, a pathological hallmark of AD, and neurotoxic A $\beta$  oligomers are formed as intermediates or off-path products of fibrillization.<sup>8</sup> The high resolution molecular structure of A $\beta$  oligomers remains mostly unknown and there is no consensus on the mechanisms of oligomerization. Inhibition of initial misfolding and aggregation of A $\beta$  peptides is considered as one of the most promising therapeutic targets for AD.<sup>8–13</sup> In this context, resolving the atomic structure of aggregation-prone states of A $\beta$  peptides and small oligomers, as well as identification of initial events in oligomerization pathways is of great importance.

Although high resolution molecular models of monomeric<sup>14–27</sup> and fibrillar<sup>28–30</sup> A $\beta$  species have been resolved under different conditions, no such information is available for A $\beta$  oligomers, mostly because of their transient nature. Also, there is no agreement on the conformational properties of monomeric species involved in initial aggregation. Solution

NMR experiments revealed that A $\beta$  monomers in aqueous solutions adopt mostly random/collapsed/extended coil conformations,<sup>14,16,19,24,25,31</sup> whereas in nonpolar environments (such as mimicking lipid membranes), their structures are characterized by substantial  $\alpha$ -helical content.<sup>18,20,26,27</sup> This suggests that A $\beta$  monomers in coiled or  $\alpha$ -helical conformations may be involved in the initial stages of oligomerization (e.g., dimerization), with following structural conversion into  $\beta$ -rich structures in larger A $\beta$  species.<sup>32–34</sup> Experimental data confirm that structural changes occur in initially unstructured A $\beta$ 1–40 (A $\beta$ 40) monomers upon oligomerization, with a substantial increase in  $\beta$ -sheet content already in dimers and its gradual increase in larger oligomers.<sup>33</sup> The possibility of  $\beta$ -sheet structural organization of A $\beta$  oligomers, including antiparallel cross- $\beta$  sheet arrangements, was demonstrated experimentally for different oligomer preparations.<sup>33,35</sup> Although it is not clear whether soluble A $\beta$  monomers with  $\beta$ -sheet structure are involved in the formation of oligomers in vivo, such a possibility was explored in theoretical studies.<sup>36–38</sup> Structural

Received: June 16, 2017

Accepted: October 26, 2017

Published: November 7, 2017

models of  $A\beta$  dimers or larger oligomers were built with  $\beta$ -sheet monomers extracted from the experimental models of amyloid fibrils<sup>38</sup> or obtained with molecular dynamics (MD) conformational sampling.<sup>36,37</sup> Experimentally, the presence of  $A\beta$  dimers in the brain was first reported a few years ago,<sup>39</sup> and their possible toxicity has been confirmed recently.<sup>40,41</sup> Although it still remains controversial whether the  $A\beta$  dimer exists in vivo and is a smallest neurotoxic agent in AD, resolving its molecular structure remains an important (and challenging) task because such information can provide molecular details of the oligomerization pathway and can be further utilized in the rational development of anti-AD drugs targeting the initial stages of aggregation of  $A\beta$  peptides.

Molecular simulations and modeling complement experiment, and can provide important insight into dynamical and structural properties of different  $A\beta$  species in situations where experimental information is not readily available, such as in the case of  $A\beta$  oligomers (see, for example, a recent review<sup>42</sup>).  $A\beta$  dimers were studied in all-atom explicit and implicit solvent MD simulations with and without ligands (such as inhibitors of aggregation or metal ions).<sup>36–38,43–49</sup> Larger oligomeric species, as well as different stages of aggregation/fibrillization of  $A\beta$  monomers and other amyloidogenic proteins, were mostly investigated with coarse-grained MD and Monte Carlo simulations.<sup>45,50–54</sup> Most of the computational studies of  $A\beta$  dimers were focused on prediction of their structural properties,<sup>36–38,48,49,54–56</sup> dimerization pathways under different conditions, including in the presence of metal ions,<sup>36,46</sup> and on possible inhibitory mechanisms of various ligands.<sup>43,44,47</sup> In most of these works, initial structures of the  $A\beta$  dimer were modeled based on the experimental solution or solid state NMR data,<sup>43,44,49</sup> or were built from  $A\beta$  monomer conformations with different structural features (such as extended  $\beta$ -sheet structural content) sampled in MD simulations.<sup>36,37,54</sup>

Because of the intrinsically disordered nature of  $A\beta$  peptides<sup>7,14</sup> characterized by conformational diversity, it is very likely that multiple distinct conformations with an elevated propensity for aggregation will be involved in the formation of initial dimeric constructs (or larger oligomers), which will possibly further undergo major conformation changes along different aggregation pathways to form metastable (e.g., oligomeric) or thermodynamically stable (e.g., fibrillar)  $A\beta$  species. This is in line with the “conformational selection” paradigm for molecular recognition<sup>57,58</sup> recently used to model  $A\beta$  dimers<sup>48</sup> and ring-shaped  $A\beta$ 1–42 ( $A\beta$ 42) oligomers.<sup>48,59</sup>

In the current study, we build structural models of the  $A\beta$ 42 dimer based on the hypothesis of the initial hydrophobic association of monomers and conformational selection mechanism of the first step of dimerization. The  $A\beta$ 42 constructs were chosen because they constitute a major component of amyloid plaques in AD and are characterized by a higher propensity for aggregation compared to the more abundant  $A\beta$ 40 monomeric species. This could make misfolding and aggregation of  $A\beta$ 42 monomers a better target for therapeutic intervention in AD. Conformational space of the  $A\beta$ 42 monomer was sampled with generalized Born/solvent area (GBSA) implicit solvent replica exchange molecular dynamics (REMD) simulations, and then representative conformations with different propensity for aggregation were selected by clustering time series of a solvent exposed surface area (SASA) of hydrophobic residues. Initial structural models of the  $A\beta$ 42 dimer were built with ZDOCK protein–protein docking software<sup>60,61</sup> from the representative conformations of

$A\beta$ 42 monomers characterized by different SASA of hydrophobic residues and secondary structure content. We also consider other structural features of monomers, such as propensity to form the Asp(D)23–Lys(K)28 salt bridge (SB). This (intra- or interpeptide) SB was observed in most of the structural models of  $A\beta$ 40 and  $A\beta$ 42 amyloid fibrils,<sup>62</sup> and it may be disrupted in neurotoxic oligomers, as follows from experimental data on SE3 conformational antibody specificity toward oligomeric  $A\beta$  species.<sup>63,64</sup> It is worth noting that the antioligomer conformational antibodies do not recognize dimeric  $A\beta$  species, possibly because the antibody-specific epitopes of the toxic  $A\beta$  oligomers have some distinctive structural features not present in the dimeric structures, in addition to solvent exposed Lys28.

Analysis of structural models of the  $A\beta$ 42 dimer proposed in this study suggests possible correlations between formation of the interpeptide interface between the central hydrophobic clusters (CHCs) and such structural characteristics of monomers as secondary structure content and propensity to form the D23–K28 SB. In particular, the CHC–CHC interface in  $\alpha$ -helical rich models of the  $A\beta$  dimer is formed only for monomers with a disrupted D23–K28 SB and thus solvent exposed Lys28. No such interface is observed for most of the dimer models with a formed D23–K28 SB or in the dimers with  $\beta$ -sheet structural content. Molecular dynamics simulations were carried out to demonstrate the stability of the interpeptide CHC–CHC interface at the microsecond ( $\mu$ s) timescale.

## 2. RESULTS

**2.1. Structural Ensemble of the  $A\beta$ 42 Monomer.** In the course of MD simulations, the initial fully extended conformation of the  $A\beta$ 42 monomer collapses toward compact structures on the timescale of a few nanoseconds. The resulting structural ensemble has a narrow distribution of the radius of gyration peaked at approximately 9.7 Å (Figure S1 of Supporting Information (SI)), compared to the 43.52 Å value of the extended conformation. The structural ensemble of the  $A\beta$ 42 monomer is characterized by a high structural diversity, as expected for this intrinsically disordered system. The monomer samples a range of conformational states with different secondary structure contents and extent of solvent exposure of hydrophilic and hydrophobic residues (Figures S2 and S3 of SI). There is also a difference in propensity to form intrapeptide salt bridges between charged residues for different parts of the MD trajectory. In the context of the current study, formation of a salt bridge between Asp(D)23 and Lys(K)28 residues is of special interest (Figure S4 of SI). The experimental data on recognition of toxic  $A\beta$  oligomers by a conformational antibody suggest that Lys28 is solvent exposed in oligomers.<sup>63,64</sup> This indicates that the D23–K28 SB may be disrupted in the toxic oligomeric species. In contrast, Lys28 forms an interpeptide SB with Asp23<sup>30</sup> or intrapeptide SB with Ala42 in the experimental models of the  $A\beta$ 42 amyloid fibril.<sup>28,29</sup> Because the conformational antibody specific to toxic oligomers does not recognize both the fibrillar and monomeric  $A\beta$  species, Lys28 may form favorable electrostatic contacts with other residues in the  $A\beta$ 42 monomer, similar to what is observed in the fibrillar  $A\beta$  structures.

The analysis of time evolution of the distance between Asp23 and Lys28 residues reveals that the MD trajectory has segments characterized by a different propensity to form the D23–K28 SB (Figure 1). In particular, the last part of the production run

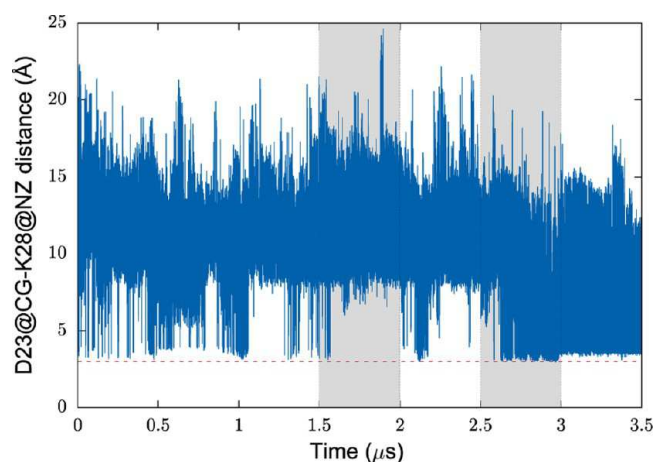


**Figure 1.** Time evolution of the distance between CG atomic site of Asp23 and NZ site of Lys28 in the REMD simulation of the  $A\beta_{42}$  monomer. The gray areas show two production segments of the trajectory used for selection of representative conformations for modeling the  $A\beta_{42}$  dimer. A segment on the left is characterized by the D23–K28 SB mostly in the off state. The right segment features transitions between on and off states, with a relatively high population of the D23–K28 SB on state. Here and below, the data are shown for the REMD replica corresponding to 25 °C.

(>2.5  $\mu\text{s}$ ) has a higher propensity compared to that of the rest of the trajectory. Because the solvent exposure of Lys28 may be one of the structural signatures of the toxic  $A\beta$  oligomers as discussed above, two segments of the MD trajectory with different propensity to form the D23–K28 SB are used in the next section to identify representative conformations of the  $A\beta_{42}$  monomer for building initial structural models of the dimer.

Despite the fact that the radius of gyration quickly relaxes to a quasi-stationary state, a root-mean-square deviation (RMSD) of atomic positions is characterized by relatively large fluctuations at the microsecond timescale (Figure 2). The time series of RMSD features two distinctive domains separated by a 4.7 Å threshold (indicated by the red dashed line in Figure 2; see also Figure S5 of SI), with a “large RMSD” domain dominating in a long run (Figure S6 of SI). The ensemble of conformations from this domain is characterized by a broader distribution of SASA for different residue groups. The SASA distribution of the hydrophobic residues, for example, is shifted toward a higher exposure compared to that of the “small RMSD” domain (Figure S7 of SI). Because of the large-scale fluctuations of RMSD at the microsecond timescale, it is not obvious whether the small RMSD domain features will reoccur in a longer simulation. On the other hand, there is a much better agreement between calculated and experimental  $J$ -coupling values if only the conformations from the large RMSD domain are used (see the discussion in the **Material and Methods** section). This suggests that this domain may describe the conformational properties of the  $A\beta_{42}$  monomer more accurately, and thus it is used for selection of representative structures of the monomer in the next section.

It is important to emphasize that using MD sampling based on the implicit solvent GBSA model may provide a conformational bias due to overestimation of specific electrostatic interactions and a higher tendency (compared to explicit solvent simulations) to form  $\alpha$ -helical structures.<sup>65,66</sup> Thus, the conformational ensemble generated in this study is charac-

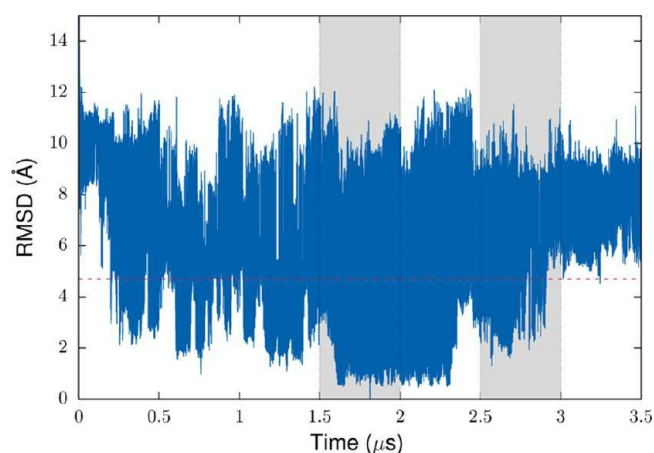


**Figure 2.** Time evolution of the  $C\alpha$  RMSD in the REMD simulation of the  $A\beta_{42}$  monomer. As a reference structure for the RMSD calculation, a structure closest to the centroid of the most populated cluster from clustering of time series of the radius of gyration was used. The radius of gyration of this structure is 9.72 Å, which is close to the value corresponding to the maximum of the radius of gyration distribution calculated for different parts of the trajectory (Figure S1 of SI). The gray areas show two segments of the trajectory used for selection of representative conformations for modeling the  $A\beta_{42}$  dimer.

terized by an elevated  $\alpha$ -helical and a reduced random coil content (Figure S2 of SI), compared to what was observed in previous all-atom explicit solvent MD studies of different  $A\beta$  monomeric species (see, for example, a recent review<sup>67</sup>). At the same time, the current REMD protocol predicts regions with a higher propensity to form different elements of secondary structures, including  $\alpha$ -helices, turns, and  $\beta$ -strands (Figure S8 of SI), in agreement with some previous MD simulations of  $A\beta$  peptides that sampled the conformational properties of  $A\beta$  peptides in agreement with experimental data.<sup>68</sup> Along with reasonable  $J$ -coupling data, this suggests that monomeric constructs selected for building initial models of the  $A\beta_{42}$  dimer may represent physiologically relevant conformations of the  $A\beta_{42}$  monomer. This is further supported by the fact that implicit solvent models can perform well in predicting structural properties of biomolecules,<sup>66,69,70</sup> including intrinsically disordered peptides and folded small peptides.<sup>66</sup>

**2.2. Selection of Representative Conformations of the  $A\beta_{42}$  Monomer.** Solvent exposure of hydrophobic residues is one of the most important factors defining aggregation propensity of amyloidogenic proteins and peptides. An increase in the extent of exposure due to changes in solvent environmental conditions (such as the level of pH, salt concentration, solvent composition, or intra-cellular crowding) may affect conformational equilibrium between different  $A\beta$  structural states by shifting the balance toward oligomeric species. Initial hydrophobic association of  $A\beta$  peptides can be followed by structural rearrangement caused by formation of specific interactions, including hydrogen bonds and salt bridges, between constituting monomers. Formation of such interactions at the earlier stages of an aggregation pathway may be impeded by a high cost of desolvation of polar and charged residues, which can be reduced after initial hydrophobic association.

In the current study, conformations of the  $A\beta_{42}$  monomer with a high solvent exposure of hydrophobic residues and their potential interaction partners are used to build initial models of

the A $\beta$ 42 dimer. These conformations were identified by clustering time series of the hydrophobic SASA (Figure 3) from

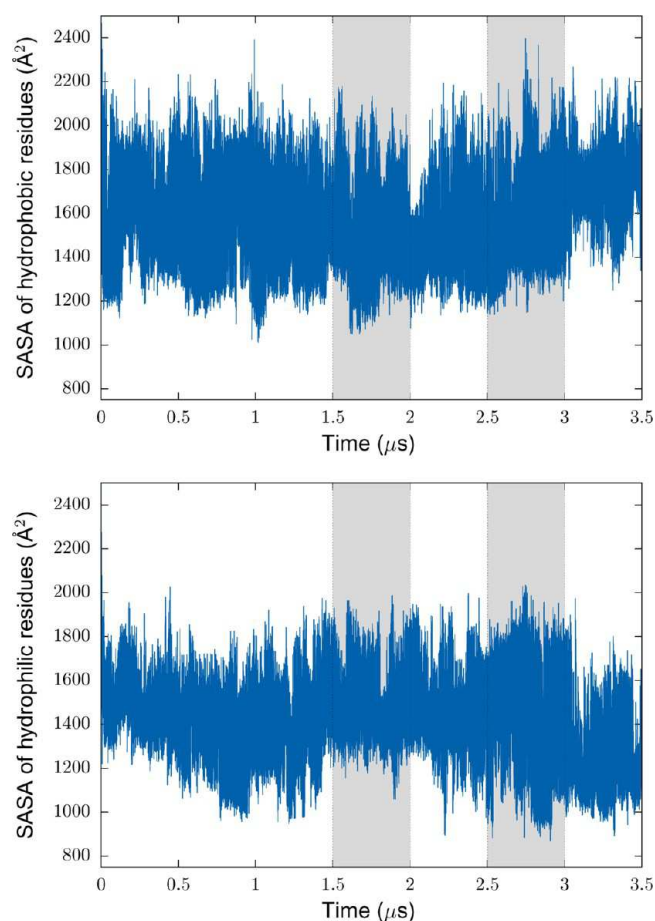


**Figure 3.** Time evolution of solvent exposed surface area (SASA) of hydrophobic (the upper panel) and hydrophilic (the bottom panel) residues of the A $\beta$ 42 monomer. The gray areas show two production segments of the trajectory.

the two production segments of the MD trajectory. Clustering was performed with the hierarchical agglomerative (bottom-up) technique<sup>71</sup> implemented in the *cptraj* program from the Amber molecular dynamics package.<sup>72</sup> Five structural clusters were identified for each production segment of the MD trajectory. Representative structures with the smallest RMSDs of C $\alpha$  atomic positions relative to the centroids of clusters with the largest hydrophobic SASA and the most populated clusters were selected for building initial structural models of the A $\beta$ 42 dimer. These structures are characterized by a substantial  $\alpha$ -helical content. This is a consequence of a relatively high population of such structures in the structural ensemble of the A $\beta$ 42 monomer sampled with the implicit solvent GBSA model. To include in the analysis conformations with other structural features, clustering of hydrophobic SASA was performed for a subset of MD frames with  $\beta$ -strand content. Selected representative structures were used to build initial models of the A $\beta$ 42 dimer, along with the  $\alpha$ -helical structures.

It is worth noting that due to the substantial memory allocation required for calculation of the matrix of pairwise distances in the parameter space, clustering could not be performed for the entire production trajectory without skipping a substantial portion of MD frames. With every second frame

omitted, clustering with the protocol described above results in identification of five representative structures with none of them having a formed D23–K28 SB. With a modified protocol set to identify 10 structural clusters, only 2 out of 10 representative structures belong to the second production section, and both of them are characterized by a formed D23–K28 SB. Among the other eight structures, there are no structures with an elevated hydrophobic SASA and a disrupted SB. Clustering of the entire trajectory may provide a more accurate representation of the population distribution of different structures in the conformational ensemble, compared to a separate clustering of two production segments of the trajectory adopted here. At the same time, using trajectory segments with different propensity to form the D23–K28 SB guarantees a structural diversity of representative conformations that are of high relevance in the context of the current study. In particular, the approach allows us to select representative structures with a high solvent exposure of hydrophobic residues with the SB both in the off and on states.

**2.2.1. Representative Conformations of the A $\beta$ 42 Monomer with  $\alpha$ -Helical Structure Content.** Conformations of the A $\beta$ 42 monomer representing the structural cluster with a large hydrophobic SASA and the most populated cluster from the first production segment of the trajectory with a low propensity to form the D23–K28 SB are shown in the top panel of Figure 4. A distinctive feature of these structures is a hydrophobic interface between the central hydrophobic cluster (residues Leu17, Val18, Phe19, and Phe20) and C-terminal hydrophobic Val40 and Ile41. It is worth noting that such contacts are absent in the A $\beta$ 40 monomer, which may partially explain differences in conformational properties and propensity for aggregation between A $\beta$ 42 and A $\beta$ 40 peptides.

The large hydrophobic SASA of the structure in the top-left panel of Figure 4 (1942 Å<sup>2</sup> compared to 1134 Å<sup>2</sup> value for the structure from the most populated cluster shown in the right panel) can be attributed to a partial solvent exposure of residues in the central hydrophobic cluster (CHC) as well as to solvent accessibility of hydrophobic Ile32 and Val36. For the structure representing the most populated cluster (the top right panel of Figure 4), residues from the CHC form hydrophobic contacts with Ile32 and Val36, which results in a decreased hydrophobic SASA. Despite a relatively small exposure of hydrophobic residues, this conformation can be considered as a good candidate to model initial hydrophobic association because of a possible reduction of the entropic penalty toward association. This is a consequence of a relatively good packing of the hydrophobic residues, which may result in reduced flexibility of this structure. Also, hydrophobic patches formed by the CHC and Ile32–Val36 domains, which are disconnected in the structure with the large hydrophobic SASA, are now merged in a large continuous patch, creating favorable conditions for hydrophobic association of monomers.

We also note that Lys28 residue, which may form an intra- or interpeptide SB in experimental models of the A $\beta$ 42 amyloid fibril and is implicated in the conformational antibody recognition of toxic oligomers,<sup>63,64</sup> is solvent exposed in all representative structures from the first production segment of the trajectory. Asp23 residue, a SB partner of Lys28 in some fibrillar structures, is solvent exposed in the most populated cluster, and is buried inside the peptide fold for the structure with the large solvent exposure of hydrophobic residues where it forms a SB with Arg5. The latter is characterized by a high propensity to form SBs with multiple residues, including Asp1,

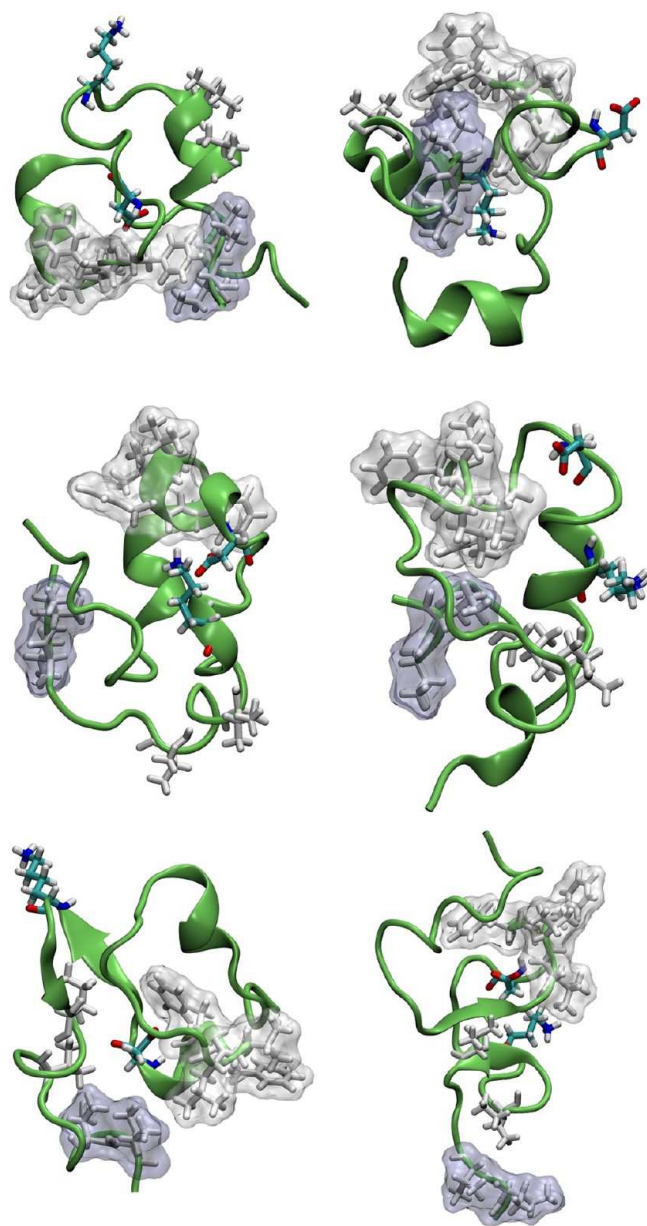


**Figure 4.** Representative conformations of the  $A\beta_{42}$  monomer with a large solvent exposure of hydrophobic residues (the left column) and from the most populated structural clusters (the right column). Top panel: structures from the first production segment of the MD trajectory characterized by a low propensity to form the D23–K28 salt bridge. Middle panel: structures from the second production segment of the trajectory characterized by a high propensity to form the salt bridge. Bottom panel: structural models of the  $A\beta_{42}$  monomer with  $\beta$ -sheet content. Asp23 and Lys28 residues are drawn in stick representation and colored according to their atom names. Hydrophobic residues from the central hydrophobic cluster (CHC), and hydrophobic Ile32, Val36, Val40, and Ile41 residues from the C-terminal part of the monomer are shown in stick representation. Transparent molecular surfaces of residues from the CHC (white color), as well as of Val40 and Ile41 residues (blue color) are also shown.

Glu3, Glu11, Glu22, and Asp23, in the representative structures from both production segments of the trajectory.

In contrast to the case of the first production segment of the trajectory where none of the representative structures had the D23–K28 SB, two out of five representative conformations

from the second segment are characterized by a formed SB. These two structures belong to the least populated structural clusters and have a relatively high solvent exposure of hydrophobic residues. In all other structures, the D23–K28 SB is disrupted and Lys28 is mostly solvent exposed. Asp23 residue is partially buried in these structures and may form a SB with Arg5, similar to the case of the first segment of the trajectory.

The representative structures from the cluster characterized by a large hydrophobic SASA and the most populated cluster from the second production part of the trajectory are shown in the middle panel of Figure 4. Their hydrophobic SASA is 2150 and 1462  $\text{\AA}^2$ , respectively. Similar to the first segment, the structure with the D23–K28 SB off state from the most populated cluster has the hydrophobic contacts between the CHC domain and the C-terminal hydrophobic residues (the middle right panel of Figure 4). What is new is that there is no hydrophobic interface between the CHC domain and C-terminal Val40 and Ile41 for the structure with the largest hydrophobic SASA. This structure is characterized by a formed D23–K28 SB (the middle left panel of Figure 4). Inspection of all representative structures from both production segments of the trajectory suggests that formation of the D23–K28 SB correlates with disruption of the hydrophobic interface between the CHC domain and C-terminal residues of the monomer.

It is worth noting that the structures with the largest hydrophobic SASA belong to the least populated structural clusters. This agrees with the notion that in aqueous environments, burying of hydrophobic residues is a thermodynamically favorable process resulting in optimization of the solvation part of a system's free energy.

**2.2.2. Representative Conformations of the  $A\beta_{42}$  Monomer with  $\beta$ -Sheet Structure Content.** The structural models of the  $A\beta_{42}$  monomer discussed above are characterized by a substantial  $\alpha$ -helical content. Most probably, this is a consequence of under-sampling of the conformational ensemble of the monomer with the implicit solvent GBSA model, resulting in a reduced population of random coil and  $\beta$ -strand structures. To address this problem in the context of probing possible dimerization pathways, and to further explore the diversity of the conformational space of the  $A\beta_{42}$  monomer, representative structures were also selected from a subset of MD frames characterized by an elevated  $\beta$ -strand structure content. As in the previous section, these structures were identified with clustering of time series of the hydrophobic SASA. Most of the selected conformations are characterized by a relatively high solvent exposure of hydrophobic residues, with the exception of one structure with a large  $\alpha$ -helical content. This structure was excluded from the following analysis because of its similarity to the structures discussed in the previous section.

The representative conformations of the  $A\beta_{42}$  monomer with  $\beta$ -strand content have a different pattern in packing of hydrophobic residues compared to that of most of the  $\alpha$ -helical structures characterized by a disrupted D23–K28 SB. In particular, there is no hydrophobic interface between the CHC domain and C-terminal hydrophobic residues, which was observed only for the  $\alpha$ -helical structures with the intrapeptide D23–K28 SB. It is worth noting that in all structures with  $\beta$ -strand content, Lys28 is solvent exposed and it does not establish a SB with Asp23. Similar to what was observed for some  $\alpha$ -helical structures, Asp23 can form a SB with Arg5.

All  $\beta$ -strand representative structures are characterized by the antiparallel  $\beta$ -sheet structural motif. The structure with the largest hydrophobic SASA (the bottom-left panel of Figure 4) has a  $\beta$ -hairpin formed by Ser26, Asn27 and Ala30, Ile31 residues. In the structure representing the most populated cluster,  $\beta$ -strands are formed by His14, Gln15 and Met35, Val36 residues (the bottom-right panel of Figure 4). The conformation with the largest exposure of hydrophobic residues (with the hydrophobic SASA of 1887 Å<sup>2</sup> compared to 1777 Å<sup>2</sup> for the structure from the most populated cluster) belongs to the third (out of five) most populated structural cluster, not to the least populated one as was observed for the  $\alpha$ -helical conformations in the previous section. This can be explained by the fact that MD frames with a particular structural feature ( $\beta$ -strand content in this case) were preselected for clustering analysis, which may affect a population balance linked to the system's free energy in unbiased ensembles.

**2.3. Structural Models of the A $\beta$ 42 Dimer.** All models of the A $\beta$ 42 dimer discussed below were generated with the ZDOCK protein–protein docking software.<sup>60,61</sup> The top 10 structures from docking simulations for each dimer model were optimized and rescored with the Amber molecular dynamics package,<sup>72</sup> as discussed in the **Material and Methods** section.

**2.3.1. Models of the A $\beta$ 42 Dimer Built from Monomeric Constructs with a High Solvent Exposure of Hydrophobic Residues.** By utilizing the hypothesis of initial hydrophobic association, in this section, structural models of the A $\beta$ 42 dimer were built from the monomeric constructs representing the structural clusters with a large hydrophobic SASA. For both production segments of the MD trajectory, monomers with a high solvent exposure of hydrophobic residues belong to the least populated clusters. This indicates that these monomeric constructs are unlikely to form initial aggregates at low physiological concentrations, but probability of dimerization may increase with increasing monomer concentration. The equilibrium balance between different monomeric structures can also be shifted toward constructs with a higher exposure of hydrophobic residues as a consequence of a change in the environmental conditions. This can make initial hydrophobic association of monomers a more likely event, as supported by some experimental data. In another scenario, monomers with a large hydrophobic SASA interact in the process of dimerization with more abundant conformations representing highly populated structural clusters characterized by a lower solvent exposure of hydrophobic residues. This possibility will be discussed in the next sections.

The top-ranked structural models of the A $\beta$ 42 dimer constructed from the monomers with a high solvent exposure of hydrophobic residues from both production segments of the trajectory are shown in Figure 5 (see also Figures S9 and S10 of SI where three top-ranked models of the dimer for each trajectory segment are shown). The interpeptide interface in all top-ranked models built with the monomer from the first segment characterized by a disrupted D23–K28 SB includes hydrophobic contacts between the CHC domains and contacts between the CHC domain of one monomer and the C-terminal hydrophobic residues of the other (the left panel of Figure 5 and Figure S9 of SI). For the second-ranked structure, there is an additional hydrophobic contact between C-terminal Ile41 residues of the monomers (the middle panel of Figure S9 of SI). The three top-ranked models represent structural properties of 8 out of 10 top-ranked dimer models built with the ZDOCK software, with the third-ranked structure (the right

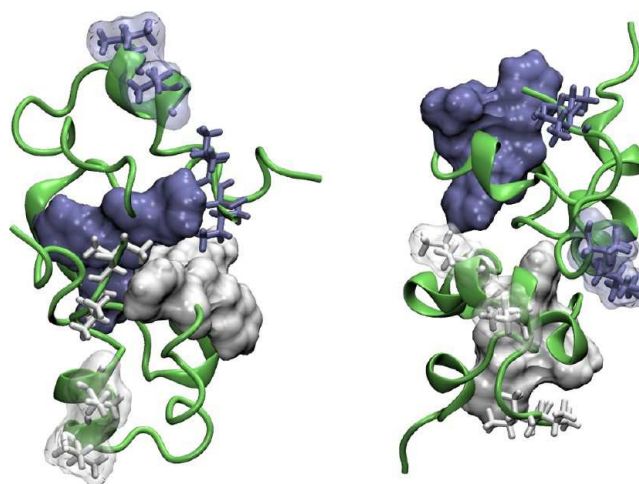


**Figure 5.** First-ranked models of the A $\beta$ 42 dimer built from the monomeric constructs with a high solvent exposure of hydrophobic residues from the first (the left panel) and the second (the right panel) production segments of the trajectory. Residues in the central hydrophobic clusters are shown by their molecular surface, hydrophobic Ile32 and Val36 and C-terminal Val40 and Ile41 are shown in stick representation, with white and blue colors used for different monomers. For the Ile32 and Val36 residues, transparent molecular surfaces are also shown.

panel of Figure S9 of SI) representing the largest structural cluster (4 out of 10 structural models).

Along with the hydrophobic interactions, there are favorable electrostatic intermonomer contacts between Asp7 and Lys16 residues for all three top-ranked structures. This may result in the formation of SBs between these residues. For the first-ranked structure, all other ionizable residues with the exception of Asp23, which may form an intrapeptide SB with Arg5, are solvent exposed and are not involved in the formation of favorable electrostatic intra- or interpeptide contacts. For the third-ranked structure, Lys16 from both monomers in the dimer can alternatively form favorable electrostatic contacts with either Glu3 or Asp1. For the second-ranked structure, there is also unfavorable electrostatic contact between Asp1 and Glu22. This indicates that this model may undergo structural changes after initial association to optimize the electrostatic interactions.

It is worth noting that the hydrophobic residues from the CHC domains and C-termini are only partially buried in the interpeptide interface in the dimer models discussed above. Residues that are not involved in formation of the interpeptide interface may form relatively large continuous hydrophobic patches. This can potentially result in further association of dimers with formation of A $\beta$ 42 tetrameric constructs and other larger oligomers.

The representative structure of the A $\beta$ 42 monomer with a high solvent exposure of hydrophobic residues from the last production segment of the trajectory is characterized by a formed D23–K28 SB. Dimer models built with this monomeric construct do not have the hydrophobic interpeptide CHC–CHC interface (the right panel of Figure 5 and Figure S10 of SI). This is different from the case of the models without the intrapeptide D23–K28 SB discussed above. Still, the top-ranked models have multiple interpeptide hydrophobic contacts. The first-ranked model, for example, has a relatively good hydrophobic interface (Figure S11 of SI) formed by a

Phe20–Val24–Val24–Phe20 “sandwich” of hydrophobic residues, as well as a hydrophobic interface between Val12, Ile31, Ile32, and Leu34 residues from both monomers.

To quantify contributions of individual residues to the interpeptide interface in dimeric constructs, we calculated average desolvation profiles of the monomers for all dimer models obtained with the ZDOCK software. A desolvation profile is defined as the difference between normalized SASAs of residues in constituting monomers and a dimer, averaged over 10 top-ranked structures for each dimer model. The dimer models with the intrapeptide D23–K28 SB in the off state (the top panel of Figure 6) are characterized by a larger decrease in solvent exposure of hydrophobic residues from the CHC domain compared to that of the models with the formed D23–K28 SB (the bottom panel of Figure 6). This suggests that there is a correlation between formation of the D23–K28 SB and a propensity to form the interpeptide CHC–CHC interface not only for the top-ranked models, but also for a

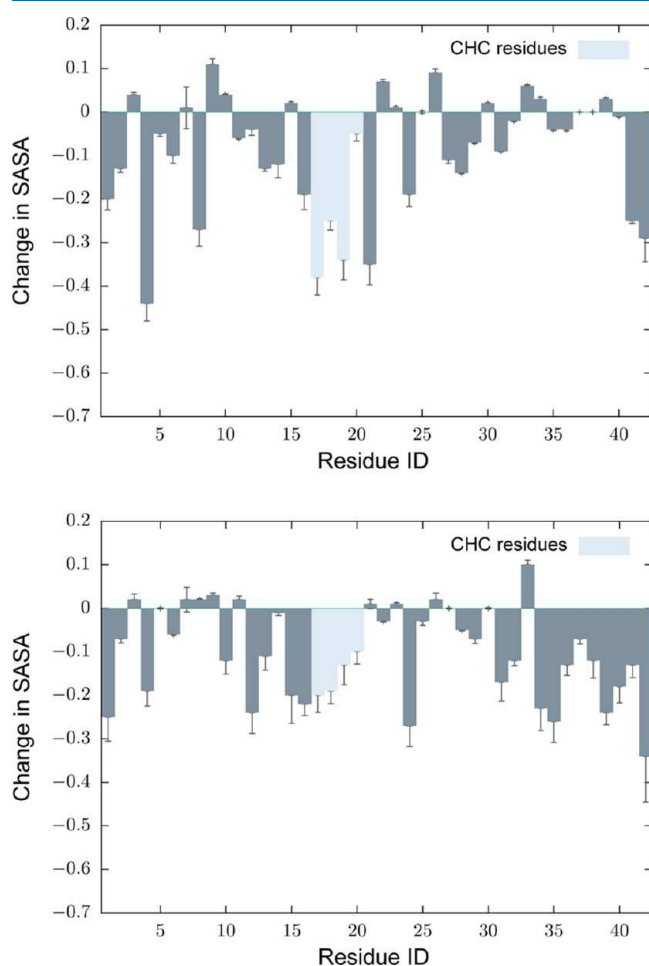


**Figure 6.** Changes in solvent accessible surface area (SASA) of individual residues upon dimerization of the  $A\beta_{42}$  monomer with a high solvent exposure of hydrophobic residues. The top and bottom panels are for the dimer models built with the monomers from the first and second production segments of the trajectory with the D23–K28 SB in the off and on states, respectively. The SASAs of individual residues are normalized relative to their values in the Gly–X–Gly tripeptide structure in a fully extended conformation. Vertical lines give standard error of means for the ten top-ranked dimer models. Contributions of residues from the CHC domain are shown with a lighter color.

structurally diverse ensemble of dimeric structures identified in docking experiments.

**2.3.2. Models of the  $A\beta_{42}$  Dimer Built with Monomeric Constructs from the Most Populated Structural Clusters.** To verify whether a hydrophobic interface between the CHC domains can form upon aggregation of monomers with a relatively low exposure of hydrophobic residues, structural models of the  $A\beta_{42}$  dimer were built with the monomeric constructs representing the most populated structural clusters. For these monomers with a disrupted D23–K28 SB, all top-ranked dimer models have interpeptide contacts between the CHC domains (Figure 7 and Figures S12 and S13 of SI). This

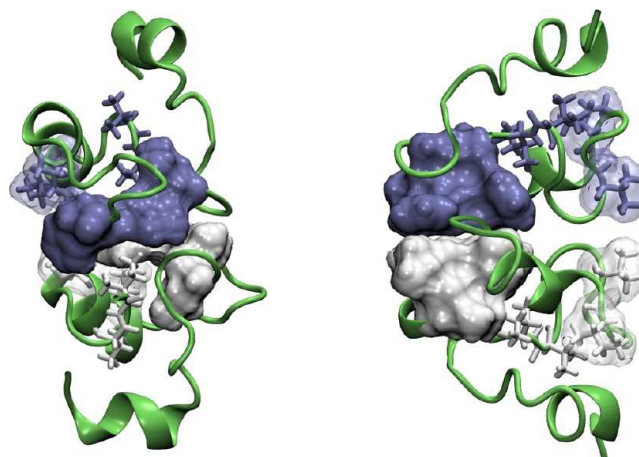


**Figure 7.** Same as in Figure 5, but for the  $A\beta_{42}$  dimer models built with the monomers representing the most populated structural clusters.

is consistent with the previous observation that monomers with a disrupted D23–K28 SB have a high propensity to form the interpeptide CHC–CHC interface. This is further confirmed by inspection of the corresponding desolvation profiles (Figure S14 of SI).

Dimers originating from the first segment of the trajectory are characterized by additional interactions between hydrophobic residues from the CHC domain of one monomer and the C-terminal domain of the other (the left panel of Figure 7 and Figure S12 of SI), which is similar to what was observed for the dimer models built from the monomer with a large hydrophobic SASA. The interpeptide interface of the first-ranked structure can be further stabilized by  $\pi$ -stacking interactions between Phe19 residues from the CHC domains. For the second-ranked structure, there is an additional hydrophobic contact between C-terminal Ile41 residues of the monomers. All of these models are characterized by a relatively high solvent exposure of hydrophilic residues and reduced exposure of hydrophobic residues, and, in contrast to the case of the dimer models built with the monomer structure with a large hydrophobic SASA, they do not have favorable interpeptide SBs.

For the final production segment of the trajectory, most of the top-ranked dimer models belong to two distinctive structural groups covering 7 out of 10 top-ranked structures (the right panel of Figure 7 and Figure S13 of SI). In addition to the hydrophobic interpeptide CHC–CHC interface, the first-ranked structure may have hydrophobic contacts between Val36 residues, and the second-ranked one between the CHC domain of one monomer and the C-terminal hydrophobic

residues of the other. The latter structure can be also stabilized by  $\pi$ -stacking interactions between Phe19 and Phe20 for both monomers.

**2.3.3. "Heterogeneous" Models of the  $A\beta$ 42 Dimer.**  $A\beta$  monomers interacting at the initial stage of dimerization most probably have different structural properties. In a likely scenario, one of the monomers with an elevated propensity for aggregation (such as resulting from a high solvent exposure of hydrophobic residues) may belong to a low-populated structural cluster, whereas its interaction partner from a highly populated cluster will have a reduced propensity for aggregation. To describe such a situation, models of the  $A\beta$ 42 dimer were built with monomers having a different degree of solvent exposure of hydrophobic residues, such as that characterized by a large hydrophobic SASA and representing the most populated structural clusters. The monomers with the large hydrophobic SASA from both production segments of the trajectory belong to the least populated structural clusters, and the monomers from the most populated clusters have a reduced hydrophobic SASA.

The dimer models originating from the first and second segments of the trajectory are compared in Figure 8 (see also

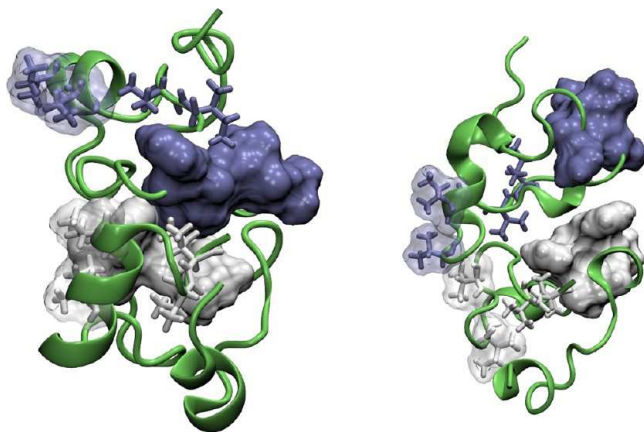


**Figure 8.** First-ranked models of the  $A\beta$ 42 dimer built with the monomeric constructs representing the most and the least populated structural clusters from the first (the left panel) and the second (the right panel) production segments of the trajectory. The monomers from the least populated clusters are characterized by a highest solvent exposure of hydrophobic residues among all the representative structures. These monomers have the D23–K28 SB in the off and on states for the dimer models shown in the left and right panels of the figure, respectively. Notations are the same as in Figure 5.

Figures S15 and S16 of SI). In the case of the first segment, both constituting monomers do not have the D23–K28 SB. Most of the corresponding dimer models (9 out of 10 top-ranked models, with the exception of the structure ranked second) are characterized by the interpeptide CHC–CHC interface. The first-ranked model has additional hydrophobic contacts between C-terminal hydrophobic residues of one monomer and the CHC domain of the other (the left panel of Figure 8). The model ranked third has a good packing of hydrophobic residues, with the hydrophobic interface formed between the CHC domains, and the CHC domain and C-terminal residues for both monomers (the right panel of Figure S15 of SI). The structure ranked second has a few hydrophobic contacts, such as between the C-terminal domains, and the C-terminal residues of one monomer and the CHC domain of the

other (the middle panel of Figure S15 of SI). Most of the models, including all three top-ranked ones, do not have favorable interpeptide electrostatic contacts.

The representative structures of the monomer from the last segment of the trajectory corresponding to the most populated cluster and having a high solvent exposure of hydrophobic residues are characterized by the D23–K28 SB in the off and on state, respectively. Most of the dimer models built with these monomeric constructs (8 out of 10, including all three top-ranked models) do not have hydrophobic contacts between the CHC domains of the monomers, in agreement with the assumption that the D23–K28 SB protects from formation of the interpeptide CHC–CHC interface. The above confirms this hypothesis for dimers in which only one of the constituting monomers has the D23–K28 SB. Even without CHC–CHC interactions, the top-ranked dimer models have multiple hydrophobic contacts between residues from other parts of the monomers. For the first-ranked model (Figure S16 of SI), for example, there are hydrophobic interactions between Leu31, Val36, and Val39 residues of the monomer from the most populated cluster, and Leu34, Met35, Val36, and Val40 residues from the monomer with a high solvent exposure of hydrophobic residues from the least populated cluster. All three top-ranked structures belong to the same structural cluster and thus show a similar pattern in hydrophobic interactions.

**2.3.4. Structural Models of the  $A\beta$ 42 Dimer Built from Monomeric Constructs with  $\beta$ -Sheet Content.** To explore possible structural features of the interpeptide interface in dimers made of monomers with  $\beta$ -sheet content, corresponding models were built by docking both identical and distinctive monomeric  $\beta$ -sheet constructs, similar to what was done in the previous sections for the  $\alpha$ -helical structures. Most of the top-ranked dimeric constructs with  $\beta$ -sheet content do not have the interpeptide CHC–CHC interface (Figure 9 and Figures S17

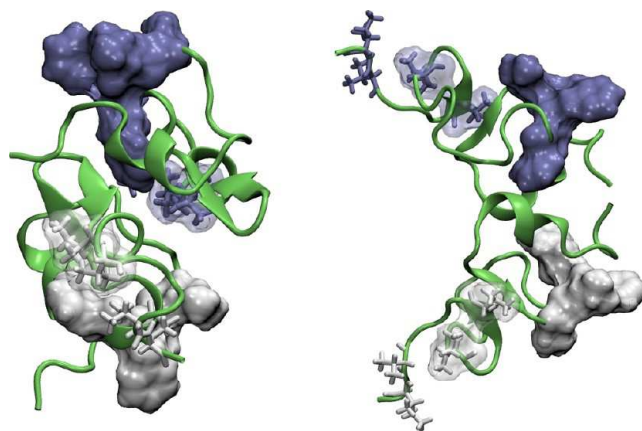


**Figure 9.** First-ranked models of the  $A\beta$ 42 dimer built from the  $\beta$ -sheet monomers representing the structural cluster characterized by a large hydrophobic SASA (the left panel) and the most populated cluster (the right panel). Notations are the same as in Figure 5.

and S18 of SI). This is different from the case of the models with a high  $\alpha$ -helical content and the intrapeptide D23–K28 SB off state. It is worth noting that the  $\beta$ -sheet monomers are characterized by a disrupted D23–K28 SB.

For the dimer model built from the monomeric construct with a large SASA of hydrophobic residues, all three top-ranked structures belong to the same structural cluster. These structures are characterized by multiple hydrophobic contacts

(such as between Ile31 and Leu34 residues of one monomer and Phe20, Val24, and Ile32 residues of the other), and they can be further stabilized by the interpeptide SB between Asp1 and Lys28. The dimer model built with the monomer from the most populated cluster is probably the least stable construct among all the structures considered in the current study. Although some hydrophobic contacts are observed for low ranking structures, all three top-ranked structures do not have any hydrophobic or favorable electrostatic contacts. Moreover, some acidic residues from both constituting monomers are located close enough to provide an electrostatic penalty for aggregation.

In the case of “heterogeneous” dimer models built with the monomers characterized by a high solvent exposure of hydrophobic residues and representing the most populated cluster, all three top-ranked structures do not have the interpeptide CHC–CHC interface. A structure ranked first (Figure S18 of SI) has a relatively good hydrophobic contact between multiple residues, such as between Phe4 and Val18 of one monomer and C-terminal Val40–Ala42 of the other, and between Val12 and Val36 of one monomer, and Phe20, Val24, Ile32, Met35, and Val36 of the other. There are no interpeptide SBs formed for this structure. The other two top-ranked structures belong to the same structural cluster. These structures do not have a good hydrophobic interface, but they can be stabilized by interpeptide SBs between Asp1 and Lys28, and between Lys16 and Asp1.

**2.4. Structural Relaxation and Dynamic Stability of Initial Dimer Models.** In solution,  $A\beta$  peptides exist in dynamic equilibrium between different conformational states, as well as between monomeric and aggregated species. Because of the long timescales involved, this cannot be directly modeled with all-atom explicit solvent simulations. In a simplified picture, formation of low-order oligomers, such as dimers, can be described as a two stage process that includes initial conformational selection with following structural relaxation and reorganization of stable oligomeric species (induced fit), and possible dissociation of less stable structures. The models of the  $A\beta$ 42 dimer from the previous section provide structural information on the initial interpeptide interface that is consistent with the conformational selection mechanism of peptide association. To model structural relaxation of initial aggregates and assess their dynamic stability, we carried out MD simulations of selected dimeric constructs (the protocol is explained in the [Material and Methods](#) section).

Simulations were performed for all three top-ranked models for each of the following systems: (i) the dimer built from the monomers with a large hydrophobic SASA and the D23–K28 SB off state (the left panel of Figure 5 and Figure S9 of SI); (ii) the dimer built from the monomers with a large hydrophobic SASA and the D23–K28 SB on state (the right panel of Figure 5 and Figure S10 of SI); (iii) the dimer built from the monomers with  $\beta$ -sheet content characterized by a large hydrophobic SASA (the left panel of Figure 9). In total, nine simulations were carried out. In the case of the dimer with the intrapeptide D23–K28 SB and the  $\beta$ -sheet dimer, there is no hydrophobic interface between the CHC domains of the monomers, which is formed in the  $\alpha$ -helical models without the SB.

In all MD simulations, no dissociation events were observed at the microsecond timescale. The arrangement of monomers in the dimer models is mostly preserved in the course of simulations, however a significant relaxation of the initial

structures and large fluctuations of the secondary structure content occur, which is indicative of a high level of structural flexibility of the  $A\beta$  dimer. Interestingly, the extent of changes (relative to the initial structure) in propensity to form different secondary structure elements depends on a particular model of the dimer (Figures S19–S21 of SI). Thus, there is a significant increase in the  $\beta$ -strand/ $\beta$ -bridge content for the dimers with the CHC–CHC interpeptide interface (the  $\alpha$ -helical models with a large hydrophobic SASA and no D23–K28 SB) (Figure 10 and the top-left panel of Figure S19 of SI). In contrast, there

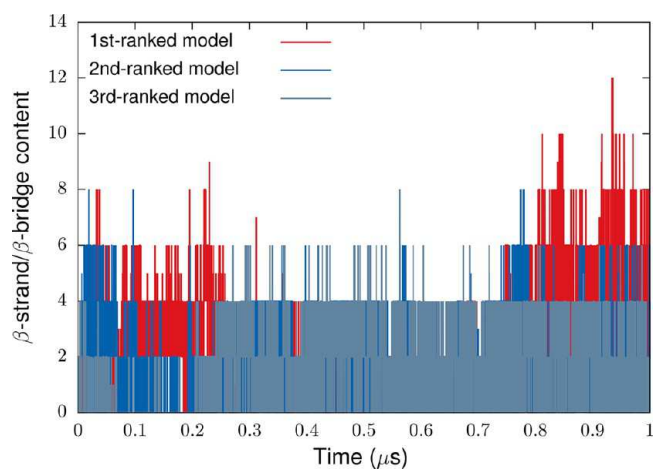


**Figure 10.** Number of residues involved in the  $\beta$ -strand/ $\beta$ -bridge structural content as a function of simulation time. The results are for the  $A\beta$ 42 dimer model built from the monomers with a large hydrophobic SASA and a disrupted D23–K28 SB. The initial structure does not have any  $\beta$ -strand/ $\beta$ -bridge content.

is no such increase for the other two dimeric models: in the case of the  $\alpha$ -helical dimer with the D23–K28 SB, the content remains negligible during the simulation (the top-left panel of Figure S20 of SI), and for the  $\beta$ -sheet dimer, it mostly fluctuates around its initial value (the top-left panel of Figure S21 of SI). Experimental data suggest that even low-order  $A\beta$  aggregates, including dimers, are characterized by an elevated  $\beta$ -sheet structural content.<sup>33</sup> The above finding may indicate that initial association of  $A\beta$  peptides involves  $\alpha$ -helical constructs with a disrupted D23–K28 SB, with following relaxation to  $\beta$ -sheet rich structures. Alternatively, there could be an equilibrium between different dimeric species under physiological conditions with the structural balance shifted (compared to the monomeric ensemble) toward  $\beta$ -sheet structures.

For two out of three simulated dimer models with the initial interpeptide CHC–CHC interface (the  $\alpha$ -helical dimer with the D23–K28 SB off state), the interface was present by the end of the simulations. Interestingly, disruption of the interface in the model ranked third correlates with establishing the intrapeptide D23–K28 SB in one of the constituting monomers (Figure 11). This suggests that the SB not only prevents formation of the initial interface between the CHC domains as discussed in the previous section, but may also control its stability in dimers after initial relaxation. It is worth noting that for the dimer models with an initially disrupted D23–K28 SB, the SB was formed only for one monomer from the third-ranked  $\alpha$ -helical dimer model.

For the first-ranked model with the initial CHC–CHC contacts between the monomers, this interface was disrupted and then re-formed at the timescale of a few hundreds of

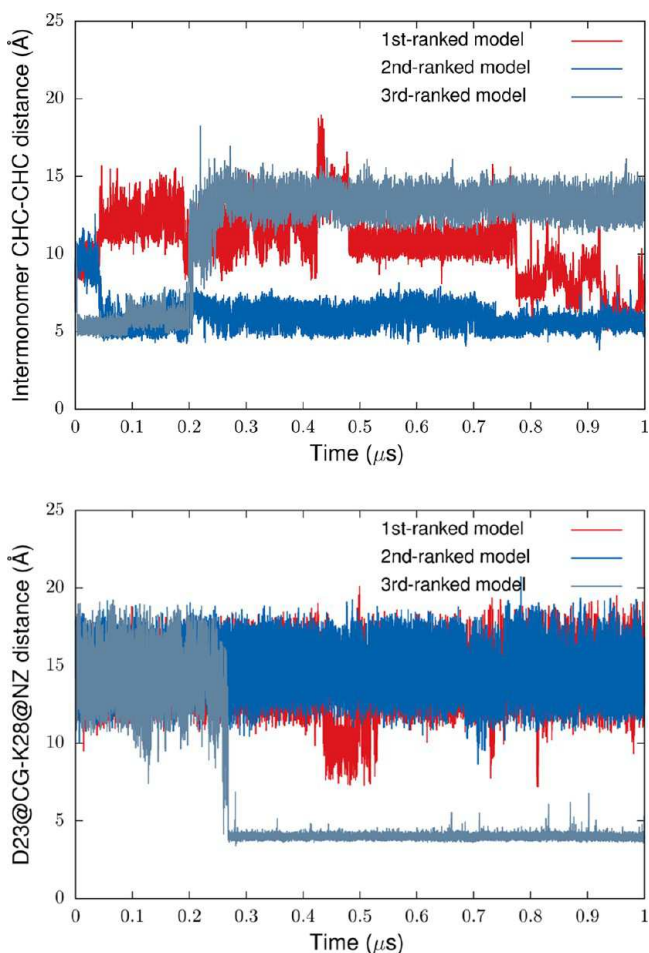


**Figure 11.** Time evolution of the interpeptide CHC–CHC distance (the upper panel) and the distance between Asp23 and Lys28 residues (the bottom panel) in the course of MD simulation of the  $A\beta$ 42 dimer. As an initial structure, the dimer model built from the monomers with a large hydrophobic SASA and the D23–K28 SB off state was used. The distances are measured between geometric centers of the CHC domains, and between the CG site of Asp23 and NZ site of Lys28.

nanoseconds. Analysis of the inter-residue distance map for this model indicates optimization of the interpeptide CHC–CHC interface in the course of simulation (Figure 12). Also, the CHC domain and adjacent residues from one of the monomers establishes better contacts with most parts of the other. Some of the initial interpeptide contacts are lost by the end of simulation, mostly between monomer termini. At the same time, constituting monomers are surprisingly stable as seen from the contact map. Thus, one of the two monomers show only minor changes in “native” contacts (the right bottom block of the distance map from Figure 12) with better packing of residues in the final structure. For the second monomer, some contacts are lost predominately between residues in termini segments and between N-terminal residues and residues 28–32. The dimer built with the  $\beta$ -sheet monomers is also characterized by a stability of the initial interpeptide interface and optimization of both inter- and intrapeptide interactions in the course of simulation (Figure 13). In contrast, for the top-ranked  $\alpha$ -helical dimer model without the CHC–CHC interface, there is a significant decrease in the initial intra- and interpeptide contacts (Figure 14). The interpeptide D23–K28 SB in these models of the  $\alpha$ -helical dimer without the CHC–CHC interface is quite stable. Its disruption was observed only for two constituting monomers from the dimer models ranked second and third. These simulations provide insight into the relative stability of structural models of the  $A\beta$ 42 dimer with and without the initial interpeptide CHC–CHC interface and also characterized by different secondary structure contents.

### 3. DISCUSSION

After being released from a lipid membrane as a product of proteolytic cleavage of APP,  $A\beta$  peptides most probably lose their  $\alpha$ -helical transmembrane conformation, as supported by solution NMR experimental data for different monomeric  $A\beta$  species in aqueous and nonpolar solutions.<sup>14–27</sup> The experimental studies have also demonstrated that soluble  $A\beta$  monomers can be classified as intrinsically disordered proteins<sup>7,14</sup> and their structural properties are characterized by transitions between multiple conformational states. It is very

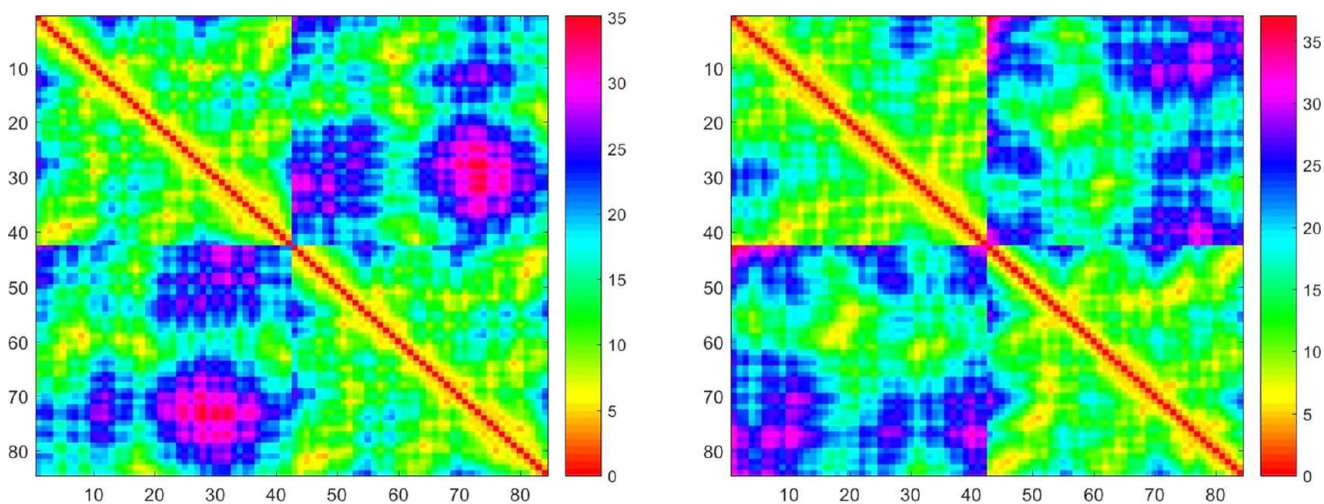


**Figure 12.** Inter-residue distance map for the first-ranked dimer model with the interpeptide CHC–CHC interface. The constituent monomers for this model characterized by a disrupted D23–K28 SB are from the first production segment of the trajectory. Left panel: the distance map for the initial structure. Right panel: the distance map averaged over the last 5 ns of 1  $\mu$ s simulation. Distances are measured between  $C\alpha$  atoms for each residue. Diagonal and off diagonal  $42 \times 42$  residue blocks give the intra- and interpeptide maps, respectively.

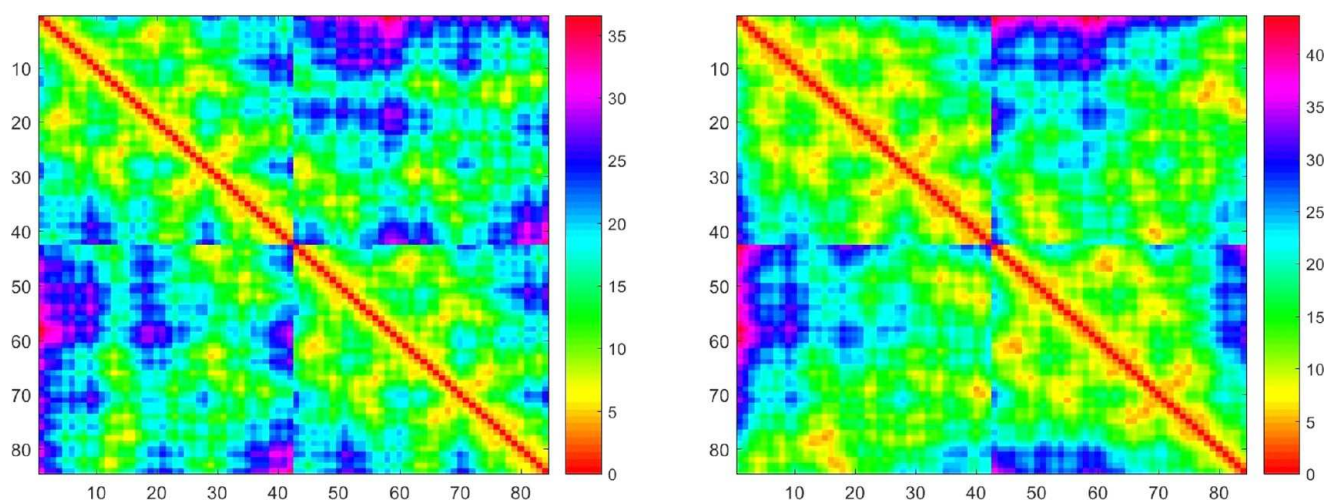


**Figure 13.** Same as in Figure 12, but for the dimer model built from the monomers with  $\beta$ -sheet content.

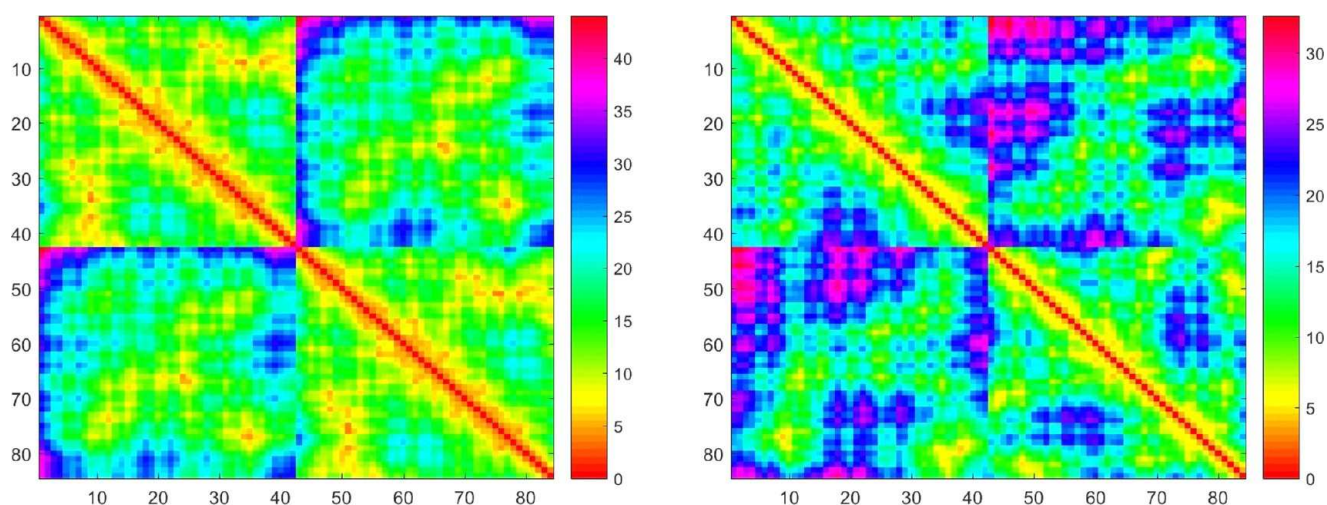


**Figure 14.** Same as in Figure 12, but for the dimer model built with the monomers from the second production segment of the trajectory. These monomers do not have the interpeptide CHC–CHC interface and are characterized by a formed D23–K28 SB.

unlikely that under normal physiological conditions, the equilibrium in the conformational ensemble of  $A\beta$  peptides is shifted toward neurotoxic oligomeric species. In a more plausible scenario, the pathological conversion is triggered by  $A\beta$  peptide overproduction, impaired clearance, or changes in environmental conditions (such as pH level, salt concentration, or presence of lipids or other substrates) caused by currently unknown pathological conditions, or a combination of these factors. The conformational equilibrium of the structural ensemble of  $A\beta$  peptides may first be shifted from mostly unstructured to  $\alpha$ -helical and/or  $\beta$ -sheet rich structures, which will further nucleate oligomerization. Such structures can be more aggregation-prone because of multiple factors, including reduced (compared to unstructured conformations) entropic penalty, a higher solvent exposure of hydrophobic residues, a favorable charge state, among others.

In this study, monomeric constructs with a potentially high propensity for aggregation were selected from the structural ensemble of the  $A\beta_{42}$  monomer sampled in implicit solvent REMD simulations. These structures are characterized by different secondary structure content, state of the D23–K28 SB, and solvent exposure of hydrophobic residues. Structural analysis suggests that there may be a correlation between

secondary structure content and propensity to form the D23–K28 SB on the one hand, and a pattern in packing of hydrophobic residues in the  $A\beta_{42}$  monomer in the other. In particular, a contact between the CHC domain and C-terminal Val40 and Ile41 residues was observed in  $\alpha$ -helical rich structures only for a disrupted D23–K28 SB. Also, there is a reduced propensity to form such contacts for structures with  $\beta$ -sheet content. These structural features of the monomer are reflected in a propensity to form the interpeptide interface between the CHC domains in models of the  $A\beta_{42}$  dimer generated with the ZDOCK protein–protein docking software.<sup>60,61</sup> There is a higher tendency to form such an interface for  $\alpha$ -helical monomers with a disrupted D23–K28 SB, compared to that of monomers with a formed SB or monomers with  $\beta$ -sheet structure content. The results of this study suggest that if the dimerization pathway involves initial association of monomers with a substantial  $\alpha$ -helical content, such monomers may have a disrupted D23–K28 SB. In this case, relaxation of initial aggregates will be accompanied by an increase in  $\beta$ -sheet content of dimers, in agreement with experimental data. Thus, formation of the intrapeptide D23–K28 SB in  $A\beta$  monomers may affect both the propensity to establish a hydrophobic

interface between CHC domains of monomers and the propensity to adopt a  $\beta$ -sheet rich conformation in dimers.

The interpeptide CHC–CHC and CHC–C-terminal domain interfaces as well as interactions between C-terminal hydrophobic residues in  $A\beta$  dimers have been observed in previous modeling studies.<sup>37,43,44,51,54</sup> What is new is that formation of such structural patterns may correlate with a propensity to form an intrapeptide D23–K28 SB and secondary structure of a monomer. This could have potential implications for better understanding of oligomerization pathways of  $A\beta$  peptides. Interactions between the CHC domain and hydrophobic Val40–Ala42 in the  $A\beta$ 42 monomer with the D23–K28 SB off state can facilitate formation of a large continuous hydrophobic patch, which could result in an elevated propensity for aggregation compared to that of  $A\beta$ 40 constructs and  $A\beta$ 42 monomers with a formed D23–K28 SB, or monomers with a substantial  $\beta$ -sheet structural content. Further, the difference in packing of hydrophobic residues between monomeric constructs with solvent exposed and protected Lys28 (such as in the case of a formed D23–K28 SB) could be a factor discriminating between aggregation pathways leading to toxic aggregates or inert fibrillar structures, as supported by the fact that solvent exposure of Lys28 is an important structural feature of the epitope recognized by the conformational antibody in the toxic oligomeric  $A\beta$  species.<sup>63,64</sup>

#### 4. CONCLUSIONS

The interplay between structural features of the  $A\beta$ 42 monomer, such as secondary structure content and a propensity to form the D23–K28 SB, and properties of the interpeptide interface in the  $A\beta$ 42 dimer identified in the current study provides a new insight into the possible oligomerization pathways of  $A\beta$  peptides. These findings are also of potential practical importance because they reveal structural features of  $A\beta$  constructs that can be utilized in development of drug candidates for inhibition of formation of toxic  $A\beta$  oligomers. In particular, they could help to identify monomeric constructs characterized by both an elevated tendency for aggregation (such as with a high solvent exposure of hydrophobic residues) and specific structural features that may be responsible for formation of toxic oligomers. These constructs can be used as receptor models for structure-based drug design or virtual screening of large libraries of druglike compounds to target pathological aggregation of  $A\beta$  peptides.

For practical applications, the above structural hypotheses need to be verified with conformational sampling covering a larger conformational space of the  $A\beta$ 42 monomer (for example, with all-atom explicit solvent MD simulations and multiple force fields to produce statistically meaningful results) combined with a combinatorial analysis of a larger number of diverse monomeric structures to build initial models of the dimer, with following assessment of dynamic and thermodynamic stability of suggested dimer models. This work is currently underway and results will be reported in forthcoming publications.

#### 5. MATERIALS AND METHODS

**5.1. Molecular Dynamics Simulations.** A conformational ensemble of the  $A\beta$ 42 monomer was sampled in GBSA implicit solvent REMD simulations. A fully extended conformation of the monomer was used as input for MD simulations to avoid a possible bias due to an arbitrary choice of initial structure. This

structure was prepared with the *tleap* program from the Amber14 molecular dynamics package.<sup>72</sup> Charge states of ionizable residues were assigned with the PROPKA program.<sup>73–75</sup> Residues with basic side chains have  $pK_a$  values greater than 10 and thus are protonated at the neutral pH conditions modeled in this study. All acidic residues are considered deprotonated because their predicted  $pK_a$  values are less than 5. PROPKA assigned the  $pK_a$  value of 6.35 to histidine residues, which provides some flexibility in assignment of their protonation states. It is very unlikely that peptides with a substantial noncompensated charge will aggregate to form a dimer. Thus, in this study focusing on building initial molecular models of the  $A\beta$ 42 dimer, all histidine residues were single-protonated at  $N\epsilon$  sites, which guaranteed electrical neutrality of monomers.

In the REMD simulations, 12 replicas spanning the temperature range 298.15–579.90 K were used. The number of replicas and temperature series were selected with the temperature generator for REMD-simulations server (<http://folding.bmc.uu.se/remd/>)<sup>76</sup> to set the replica exchange probability to 0.2. Simulations were performed with the Amber12 molecular dynamics package<sup>77</sup> and the Amber ff12SB force field.<sup>78,79</sup> A modified version of the GB solvation model<sup>80</sup> ( $igb = 5$ ) was used with the *mbondi2* set of van der Waals radii.<sup>80</sup> The ionic strength of solvent was set to 0.2 M (saltcon = 0.2) to mimic physiological conditions. To control temperature, Langevin dynamics was used with the collision frequency of 5 ps<sup>-1</sup>. All bonds that include hydrogen atoms were constrained with the SHAKE algorithm.<sup>81</sup> The cutoff parameters for non-bonded interactions and pairwise summation for calculating the effective Born radii were set to 999.0 Å.

The REMD simulations were preceded by structure optimization to relax possible steric clashes, followed by thermalization and equilibration runs. Minimization was performed with 250 steepest descent steps followed by 250 conjugate gradient minimization steps. In the thermalization run, temperature of the system was gradually increased to target temperatures for each replica during 50 000 MD steps. Thermalization was followed by 50 000 MD equilibration steps. In the equilibration and thermalization runs, the same MD parameters were used as in the production simulations with the exception of the time step which was set to 1 fs in the thermalization and equilibration runs, and to 2 fs in the production runs. In the production REMD simulations, the number of MD steps between attempted replica exchanges was 2500. To avoid possible chirality inversions at high temperatures, chirality restraints generated with the *makeCHIR\_RST* program from the Amber molecular dynamics package were imposed in the REMD simulations. All other parameters were set to their default values.<sup>72</sup>

A similar MD setup was used to assess dynamical stability of select models of the  $A\beta$ 42 dimer. These models were built and optimized as explained in the next section. To avoid dissociation of the dimers at high temperatures accessible in REMD simulations, their stability was tested with conventional MD at a temperature of 25 °C.

Before it was used to sample a conformational ensemble of the  $A\beta$ 42 monomer, the REMD protocol described above was validated by folding the Trp-cage miniprotein<sup>82</sup> starting from a fully extended initial conformation. The miniprotein was successfully folded on the nanosecond timescale (Figures S22 and S23 of SI) with the same set of REMD parameters as that used for simulation of the  $A\beta$  monomer (with the exception of

the number of replicas, which was set to 10 to insure the same exchange rates for the 20-residue long miniprotein).

In silico conformational sampling of intrinsically disordered peptides is a challenging problem. Sampling results are very sensitive to the choice of a force field model,<sup>83</sup> and it is not clear whether explicit solvent simulations can be fully converged (such as to reproduce physiological ensembles of  $A\beta$  peptides) at the microsecond timescale accessed in most studies carried out so far. Here, REMD is used to generate a structurally diverse ensemble of conformations of the  $A\beta$ 42 monomer for modeling a possible initial interpeptide interface in the  $A\beta$ 42 dimer. In this context, it is more important to produce  $A\beta$  conformations with structural characteristics related to a high propensity for aggregation rather than to achieve a converged conformational sampling. Still, it is interesting to verify whether the sampling protocol from this study generates a conformational ensemble of  $A\beta$  monomers in agreement with experimental data. With that in mind, we compare predicted  $^3J_{\text{HNH}\alpha}$ -coupling values with the recent experimental solution NMR data.<sup>14</sup> The calculation was carried out based on the modified Vuister and Bax parametrization<sup>84</sup> of the Karplus equation<sup>85–87</sup> by averaging  $J$ -coupling values for individual MD frames. The agreement between the experimental and predicted data is reasonably good for a subset of frames from the last 2  $\mu\text{s}$  of the trajectory corresponding to the large RMSD structural domain discussed above (Figure S24 of SI). Thus, the correlation coefficient between the calculated and experimental  $J$ -coupling values is 0.529, which is comparable to the previously reported results obtained with explicit solvent REMD simulations.<sup>22</sup>

**5.2. Postprocessing of Molecular Dynamics Data and Building Models of the  $A\beta$ 42 Dimer.** The conformational space of the  $A\beta$  monomer is quite complex. Thus, different criteria may be needed to identify conformers with a potentially high tendency for aggregation. In the current study, solvent exposure of hydrophobic residues was chosen as a major descriptor of the monomer's propensity for aggregation. To model an initial interpeptide interface in the  $A\beta$  dimer, representative conformations of the  $A\beta$ 42 monomer were selected with clustering of time series of solvent accessible surface area of hydrophobic residues. SASA of different residue groups and secondary structure content of peptides were obtained with Kabsch and Sander's DSSP algorithm.<sup>88</sup> All other postprocessing tasks, including clustering analysis and calculations of RMSD of atomic positions, radius of gyration, and the distance between salt-bridge forming residues, were performed with the *cptraj* program from the Amber molecular dynamics package.

Molecular models of the  $A\beta$ 42 dimer were built from the representative conformations of the monomer with the ZDOCK protein docking server (<http://zdock.umassmed.edu/>).<sup>60</sup> The server is based on the protein–protein rigid-body docking programs ZDOCK and M–ZDOCK.<sup>61,89,90</sup> The top 10 structures from each docking simulation were further optimized and rescored with the Amber molecular dynamics package and the Amber ff14SB force field.<sup>79</sup> Minimization was performed with 500 steepest descent steps followed by 500 conjugate gradient minimization steps. Minimization and rescoring of dimer models built with the ZDOCK server were performed with the same set of parameters as that used for REMD simulations.

## ■ ASSOCIATED CONTENT

### § Supporting Information

The Supporting Information is available free of charge on the ACS Publications website at DOI: 10.1021/acsomega.7b00805.

Time evolution and distribution of the radius of gyration of the  $A\beta$ 42 monomer from implicit solvent REMD simulations; solvent accessible surface area of hydrophobic residues of the  $A\beta$ 42 monomer plotted versus number of residues forming different secondary structure elements, the distance between salt-bridge forming Asp23 and Lys28 residues, and hydrophilic SASA; population distributions of  $C\alpha$  RMSD for different trajectory segments; time series of  $C\alpha$  RMSD split into two structural domains, and distribution of the hydrophobic and hydrophilic SASA of the  $A\beta$ 42 monomer for different RMSD domains; per-residue secondary structure propensity of the  $A\beta$ 42 monomer; top-ranked models of the  $A\beta$ 42 dimer built from different monomeric constructs; changes in SASA of individual residues upon dimerization of the  $A\beta$ 42 monomers from the most populated clusters; number of residues forming different secondary structure elements as a function of simulation time for different dimer models; time series of  $C\alpha$  RMSD from REMD folding simulation of the Trp-cage miniprotein; representative structures of the Trp-cage miniprotein folded in REMD simulations; comparison between calculated and experimental  $J$ -coupling data for the  $A\beta$ 42 monomer (PDF)

## ■ AUTHOR INFORMATION

### Corresponding Author

\*E-mail: [nblinov@ualberta.ca](mailto:nblinov@ualberta.ca). Phone: +1 (780)641 1719. Fax: +1 (780) 641 1601.

### ORCID

Nikolay Blinov: 0000-0003-2638-8376

Andriy Kovalenko: 0000-0001-5033-4314

### Notes

The authors declare no competing financial interest.

## ■ ACKNOWLEDGMENTS

This work was supported by the Alberta Prion Research Institute, Alzheimer Society of Alberta and Northwest Territories (Alberta Alzheimer Research Program grants ABIBS AARP 201500003 and 201600005), and the National Research Council of Canada. Computational resources were provided by WestGrid ([www.westgrid.ca](http://www.westgrid.ca)) and Compute Canada - Calcul Canada ([www.computecanada.ca](http://www.computecanada.ca)).

## ■ REFERENCES

- (1) Hardy, J.; Selkoe, D. J. The Amyloid Hypothesis of Alzheimer's Disease: Progress and Problems on the Road to Therapeutics. *Science* **2002**, *297*, 353–356.
- (2) Walsh, D. M.; Selkoe, D. J.  $A\beta$  Oligomers - a decade of discovery. *J. Neurochem.* **2007**, *101*, 1172–1184.
- (3) Benilova, I.; Karran, E.; De Strooper, B. The toxic  $A\beta$  oligomer and Alzheimer's disease: an emperor in need of clothes. *Nat. Neurosci.* **2012**, *15*, 349–357.
- (4) Kaye, R.; Lasagna-Reeves, C. A. Molecular Mechanisms of Amyloid Oligomers Toxicity. *J. Alzheimer's Dis.* **2013**, *33*, S67–S78.
- (5) Haass, C.; Selkoe, D. J. Soluble protein oligomers in neurodegeneration: lessons from the Alzheimer's amyloid  $\beta$ -peptide. *Nat. Rev. Mol. Cell Biol.* **2007**, *8*, 101–112.

- (6) Glabe, C. G. Structural Classification of Toxic Amyloid Oligomers. *J. Biol. Chem.* **2008**, *283*, 29639–29643.
- (7) Hubin, E.; van Nuland, N. A. J.; Broersen, K.; Pauwels, K. Transient dynamics of A $\beta$  contribute to toxicity in Alzheimer's disease. *Cell. Mol. Life Sci.* **2014**, *71*, 3507–3521.
- (8) Necula, M.; Kaye, R.; Milton, S.; Glabe, C. G. Small Molecule Inhibitors of Aggregation Indicate That Amyloid  $\beta$  Oligomerization and Fibrillization Pathways Are Independent and Distinct. *J. Biol. Chem.* **2007**, *282*, 10311–10324.
- (9) Walsh, D. M.; Townsend, M.; Podlisny, M. B.; Shankar, G. M.; Fadeeva, J. V.; Agnaf, O. E.; Hartley, D. M.; Selkoe, D. J. Certain Inhibitors of Synthetic Amyloid  $\beta$ -Peptide (A $\beta$ ) Fibrillogenesis Block Oligomerization of Natural A $\beta$  and Thereby Rescue Long-Term Potentiation. *J. Neurosci.* **2005**, *25*, 2455–2462.
- (10) Wang, Z.; Chang, L.; Klein, W. L.; Thatcher, G. R. J.; Venton, D. L. Per-6-substituted-per-6-deoxy  $\beta$ -cyclodextrins Inhibit the Formation of  $\beta$ -Amyloid Peptide Derived Soluble Oligomers. *J. Med. Chem.* **2004**, *47*, 3329–3333.
- (11) Fradinger, E. A.; Monien, B. H.; Urbanc, B.; Lomakin, A.; Tan, M.; Li, H.; Spring, S. M.; Condrón, M. M.; Cruz, L.; Xie, C.-W.; et al. C-terminal peptides coassemble into A $\beta$ 42 oligomers and protect neurons against A $\beta$ 42-induced neurotoxicity. *Proc. Natl. Acad. Sci. U.S.A.* **2008**, *105*, 14175–14180.
- (12) Yang, F.; Lim, G. P.; Begum, A. N.; Ubeda, O. J.; Simmons, M. R.; Ambegaokar, S. S.; Chen, P. P.; Kaye, R.; Glabe, C. G.; Frautschy, S. A.; et al. Curcumin Inhibits Formation of Amyloid  $\beta$  Oligomers and Fibrils, Binds Plaques, and Reduces Amyloid in Vivo. *J. Biol. Chem.* **2005**, *280*, 5892–5901.
- (13) Feng, B. Y.; Toyama, B. H.; Wille, H.; Colby, D. W.; Collins, S. R.; May, B. C. H.; Prusiner, S. B.; Weissman, J.; Shoichet, B. K. Small-molecule aggregates inhibit amyloid polymerization. *Nat. Chem. Biol.* **2008**, *4*, 197–199.
- (14) Roche, J.; Shen, Y.; Lee, J. H.; Ying, J.; Bax, A. Monomeric A $\beta$ 1-40 and A $\beta$ 1-42 Peptides in Solution Adopt Very Similar Ramachandran Map Distributions That Closely Resemble Random Coil. *Biochemistry* **2016**, *55*, 762–775.
- (15) Ball, K. A.; Phillips, A. H.; Nerenberg, P. S.; Fawzi, N. L.; Wemmer, D. E.; Head-Gordon, T. Homogeneous and Heterogeneous Tertiary Structure Ensembles of Amyloid- $\beta$  Peptides. *Biochemistry* **2011**, *50*, 7612–7628.
- (16) Yamaguchi, T.; Matsuzaki, K.; Hoshino, M. Transient formation of intermediate conformational states of amyloid- $\beta$  peptide revealed by heteronuclear magnetic resonance spectroscopy. *FEBS Lett.* **2011**, *585*, 1097–1102.
- (17) Vivekanandan, S.; Brender, J. R.; Lee, S. Y.; Ramamoorthy, A. A partially folded structure of amyloid-beta(1-40) in an aqueous environment. *Biochem. Biophys. Res. Commun.* **2011**, *411*, 312–316.
- (18) Tomaselli, S.; Esposito, V.; Vangone, P.; van Nuland, N. A. J.; Bonvin, A. M. J. J.; Guerrini, R.; Tancredi, T.; Temussi, P. A.; Picone, D. The  $\alpha$ -to- $\beta$  Conformational Transition of Alzheimer's A $\beta$ -(1-42) Peptide in Aqueous Media is Reversible: A Step by Step Conformational Analysis Suggests the Location of  $\beta$  Conformation Seeding. *ChemBioChem* **2006**, *7*, 257–267.
- (19) Hou, L.; Shao, H.; Zhang, Y.; Li, H.; Menon, N. K.; Neuhaus, E. B.; Brewer, J. M.; Byeon, I.-J. L.; Ray, D. G.; Vitek, M. P.; et al. Solution NMR Studies of the A $\beta$ (1-40) and A $\beta$ (1-42) Peptides Establish that the Met35 Oxidation State Affects the Mechanism of Amyloid Formation. *J. Am. Chem. Soc.* **2004**, *126*, 1992–2005.
- (20) Crescenzi, O.; Tomaselli, S.; Guerrini, R.; Salvadori, S.; D'Ursi, A. M.; Temussi, P. A.; Picone, D. Solution structure of the Alzheimer amyloid  $\beta$ -peptide (1-42) in an apolar microenvironment. *Eur. J. Biochem.* **2002**, *269*, 5642–5648.
- (21) Yan, Y.; Wang, C. A $\beta$ 42 is More Rigid than A $\beta$ 40 at the C Terminus: Implications for A $\beta$  Aggregation and Toxicity. *J. Mol. Biol.* **2006**, *364*, 853–862.
- (22) Rosenman, D. J.; Connors, C. R.; Chen, W.; Wang, C.; García, A. E. A $\beta$  Monomers Transiently Sample Oligomer and Fibril-Like Configurations: Ensemble Characterization Using a Combined MD/NMR Approach. *J. Mol. Biol.* **2013**, *425*, 3338–3359.
- (23) Hoyer, W.; Grönwall, C.; Jonsson, A.; Ståhl, S.; Härd, T. Stabilization of a  $\beta$ -hairpin in monomeric Alzheimer's amyloid- $\beta$  peptide inhibits amyloid formation. *Proc. Natl. Acad. Sci. U.S.A.* **2008**, *105*, 5099–5104.
- (24) Zhang, S.; Iwata, K.; Lachenmann, M.; Peng, J.; Li, S.; Stimson, E.; Lu, Y.; Felix, A.; Maggio, J.; Lee, J. The Alzheimer's Peptide A $\beta$  Adopts a Collapsed Coil Structure in Water. *J. Struct. Biol.* **2000**, *130*, 130–141.
- (25) Lee, J. P.; Stimson, E. R.; Ghilardi, J. R.; Mantyh, P. W.; Lu, Y.-A.; Felix, A. M.; Llanos, W.; Behbin, A.; Cummings, M.; Crielunge, M. V.; et al. 1H NMR of A $\beta$  Amyloid Peptide Congeners in Water Solution. Conformational Changes Correlate with Plaque Competence. *Biochemistry* **1995**, *34*, 5191–5200.
- (26) Talafous, J.; Marcinowski, K. J.; Klopman, G.; Zagorski, M. G. Solution Structure of Residues 1-28 of the Amyloid  $\beta$ -Peptide. *Biochemistry* **1994**, *33*, 7788–7796.
- (27) Barrow, C. J.; Zagorski, M. Solution structures of  $\beta$  peptide and its constituent fragments: relation to amyloid deposition. *Science* **1991**, *253*, 179–182.
- (28) Xiao, Y.; Ma, B.; McElheny, D.; Parthasarathy, S.; Long, F.; Hoshi, M.; Nussinov, R.; Ishii, Y. A $\beta$ (1-42) fibril structure illuminates self-recognition and replication of amyloid in Alzheimer's disease. *Nat. Struct. Mol. Biol.* **2015**, *22*, 499–505.
- (29) Wälti, M. A.; Ravotti, F.; Arai, H.; Glabe, C. G.; Wall, J. S.; Böckmann, A.; Güntert, P.; Meier, B. H.; Riek, R. Atomic-resolution structure of a disease-relevant A $\beta$ (1-42) amyloid fibril. *Proc. Natl. Acad. Sci. U.S.A.* **2016**, *113*, E4976–E4984.
- (30) Lührs, T.; Ritter, C.; Adrian, M.; Riek-Loher, D.; Bohrmann, B.; Döbeli, H.; Schubert, D.; Riek, R. 3D structure of Alzheimer's amyloid- $\beta$ (1-42) fibrils. *Proc. Natl. Acad. Sci. U.S.A.* **2005**, *102*, 17342–17347.
- (31) Riek, R.; Güntert, P.; Döbeli, H.; Wipf, B.; Wüthrich, K. NMR studies in aqueous solution fail to identify significant conformational differences between the monomeric forms of two Alzheimer peptides with widely different plaque-competence, A $\beta$ (1-40)<sup>ox</sup> and A $\beta$ (1-42)<sup>ox</sup>. *Eur. J. Biochem.* **2001**, *268*, S930–S936.
- (32) Kirkitadze, M. D.; Condrón, M. M.; Teplow, D. B. Identification and characterization of key kinetic intermediates in amyloid  $\beta$ -protein fibrillogenesis. *J. Mol. Biol.* **2001**, *312*, 1103–1119.
- (33) Ono, K.; Condrón, M. M.; Teplow, D. B. Structure-neurotoxicity relationships of amyloid  $\beta$ -protein oligomers. *Proc. Natl. Acad. Sci. U.S.A.* **2009**, *106*, 14745–14750.
- (34) Misra, P.; Kodali, R.; Chemuru, S.; Kar, K.; Wetzel, R. Rapid  $\alpha$ -oligomer formation mediated by the A $\beta$  C terminus initiates an amyloid assembly pathway. *Nat. Commun.* **2016**, *7*, No. 12419.
- (35) Stroud, J. C.; Liu, C.; Teng, P. K.; Eisenberg, D. Toxic fibrillar oligomers of amyloid- $\beta$  have cross- $\beta$  structure. *Proc. Natl. Acad. Sci. U.S.A.* **2012**, *109*, 7717–7722.
- (36) Xu, L.; Shan, S.; Chen, Y.; Wang, X.; Nussinov, R.; Ma, B. Coupling of Zinc-Binding and Secondary Structure in Nonfibrillar A $\beta$ 40 Peptide Oligomerization. *J. Chem. Inf. Model.* **2015**, *55*, 1218–1230.
- (37) Tarus, B.; Tran, T. T.; Nasica-Labouze, J.; Sterpone, F.; Nguyen, P. H.; Derreumaux, P. Structures of the Alzheimer's Wild-Type A $\beta$ 1-40 Dimer from Atomistic Simulations. *J. Phys. Chem. B* **2015**, *119*, 10478–10487.
- (38) Yano, A.; Okamoto, A.; Nomura, K.; Higai, S.; Kurita, N. Difference in dimer conformation between amyloid- $\beta$ (1-42) and (1-43) proteins: Replica exchange molecular dynamics simulations in water. *Chem. Phys. Lett.* **2014**, *595–596*, 242–249.
- (39) Shankar, G. M.; Li, S.; Mehta, T. H.; Garcia-Munoz, A.; Shepardson, N. E.; Smith, I.; Brett, F. M.; Farrell, M. A.; Rowan, M. J.; Lemere, C. A.; et al. Amyloid- $\beta$  protein dimers isolated directly from Alzheimer's brains impair synaptic plasticity and memory. *Nat. Med.* **2008**, *14*, 837–842.
- (40) O'Malley, T. T.; Oktaviani, N. A.; Zhang, D.; Lomakin, A.; O'Nuallain, B.; Linse, S.; Benedek, G. B.; Rowan, M. J.; Mulder, F. A. A.; Walsh, D. M. A $\beta$  dimers differ from monomers in structural propensity, aggregation paths and population of synaptotoxic assemblies. *Biochem. J.* **2014**, *461*, 413–426.

- (41) Yang, T.; Li, S.; Xu, H.; Walsh, D. M.; Selkoe, D. J. Large Soluble Oligomers of Amyloid  $\beta$ -Protein from Alzheimer Brain Are Far Less Neuroactive Than the Smaller Oligomers to Which They Dissociate. *J. Neurosci.* **2017**, *37*, 152–163.
- (42) Nasica-Labouze, J.; Nguyen, P. H.; Sterpone, F.; Berthoumieu, O.; Buchete, N.-V.; Côté, S.; De Simone, A.; Doig, A. J.; Faller, P.; Garcia, A.; et al. Amyloid  $\beta$  Protein and Alzheimer's Disease: When Computer Simulations Complement Experimental Studies. *Chem. Rev.* **2015**, *115*, 3518–3563.
- (43) Zhang, T.; Xu, W.; Mu, Y.; Derreumaux, P. Atomic and Dynamic Insights into the Beneficial Effect of the 1,4-Naphthoquinon-2-yl-L-tryptophan Inhibitor on Alzheimer's  $A\beta$ 1-42 Dimer in Terms of Aggregation and Toxicity. *ACS Chem. Neurosci.* **2014**, *5*, 148–159.
- (44) Zhang, T.; Zhang, J.; Derreumaux, P.; Mu, Y. Molecular Mechanism of the Inhibition of EGCG on the Alzheimer  $A\beta$ 1-42 Dimer. *J. Phys. Chem. B* **2013**, *117*, 3993–4002.
- (45) Xu, L.; Chen, Y.; Wang, X. Assembly of Amyloid  $\beta$  Peptides in the Presence of Fibril Seeds: One-Pot Coarse-Grained Molecular Dynamics Simulations. *J. Phys. Chem. B* **2014**, *118*, 9238–9246.
- (46) Pan, L.; Patterson, J. C. Molecular Dynamics Study of  $Zn(A\beta)$  and  $Zn(A\beta)_2$ . *PLoS One* **2013**, *8*, No. e70681.
- (47) Sun, Y.; Qian, Z.; Wei, G. The inhibitory mechanism of a fullerene derivative against amyloid- $\beta$  peptide aggregation: an atomistic simulation study. *Phys. Chem. Chem. Phys.* **2016**, *18*, 12582–12591.
- (48) Tsigelny, I. F.; Sharikov, Y.; Kouznetsova, V. L.; Greenberg, J. P.; Wrasidlo, W.; Gonzalez, T.; Desplats, P.; Michael, S. E.; Trejo-Morales, M.; Overk, C. R.; et al. Structural Diversity of Alzheimer's Disease Amyloid- $\beta$  Dimers and Their Role in Oligomerization and Fibril Formation. *J. Alzheimer's Dis.* **2014**, *39*, 583–600.
- (49) Blinov, N.; Dorosh, L.; Wishart, D.; Kovalenko, A. Association Thermodynamics and Conformational Stability of  $\beta$ -Sheet Amyloid  $\beta$ (17-42) Oligomers: Effects of E22Q (Dutch) Mutation and Charge Neutralization. *Biophys. J.* **2010**, *98*, 282–296.
- (50) Morriss-Andrews, A.; Shea, J.-E. Computational Studies of Protein Aggregation: Methods and Applications. *Annu. Rev. Phys. Chem.* **2015**, *66*, 643–666.
- (51) Chiricotto, M.; Tran, T. T.; Nguyen, P. H.; Melchionna, S.; Sterpone, F.; Derreumaux, P. Coarse-grained and All-atom Simulations towards the Early and Late Steps of Amyloid Fibril Formation. *Isr. J. Chem.* [Online] **2016**. <http://dx.doi.org/10.1002/ijch.201600048> (accessed July 17, 2017).
- (52) Meral, D.; Urbanc, B. Discrete Molecular Dynamics Study of Oligomer Formation by N-Terminally Truncated Amyloid  $\beta$ -Protein. *J. Mol. Biol.* **2013**, *425*, 2260–2275.
- (53) Urbanc, B.; Betnel, M.; Cruz, L.; Bitan, G.; Teplow, D. B. Elucidation of Amyloid  $\beta$ -Protein Oligomerization Mechanisms: Discrete Molecular Dynamics Study. *J. Am. Chem. Soc.* **2010**, *132*, 4266–4280.
- (54) Côté, S.; Laghaei, R.; Derreumaux, P.; Mousseau, N. Distinct Dimerization for Various Alloforms of the Amyloid-Beta Protein:  $A\beta$ 1-40,  $A\beta$ 1-42, and  $A\beta$ 1-40(D23N). *J. Phys. Chem. B* **2012**, *116*, 4043–4055.
- (55) Takeda, T.; Klimov, D. K. Interpeptide interactions induce helix to strand structural transition in  $A\beta$  peptides. *Proteins: Struct., Funct., Bioinf.* **2009**, *77*, 1–13.
- (56) Kim, S.; Takeda, T.; Klimov, D. K. Mapping Conformational Ensembles of  $A\beta$  Oligomers in Molecular Dynamics Simulations. *Biophys. J.* **2010**, *99*, 1949–1958.
- (57) Boehr, D. D.; Nussinov, R.; Wright, P. E. The role of dynamic conformational ensembles in biomolecular recognition. *Nat. Chem. Biol.* **2009**, *5*, 789–796.
- (58) Carlson, H. A. Protein flexibility and drug design: how to hit a moving target. *Curr. Opin. Chem. Biol.* **2002**, *6*, 447–452.
- (59) Tran, L.; Basdevant, N.; Prévost, C.; Ha-Duong, T. Structure of ring-shaped  $A\beta$ 42 oligomers determined by conformational selection. *Sci. Rep.* **2016**, *6*, No. 21429.
- (60) Pierce, B. G.; Wiehe, K.; Hwang, H.; Kim, B.-H.; Vreven, T.; Weng, Z. ZDOCK server: interactive docking prediction of protein-protein complexes and symmetric multimers. *Bioinformatics* **2014**, *30*, 1771–1773.
- (61) Pierce, B. G.; Hourai, Y.; Weng, Z. Accelerating Protein Docking in ZDOCK Using an Advanced 3D Convolution Library. *PLoS One* **2011**, *6*, No. e24657.
- (62) Tycko, R. Molecular Structure of Aggregated Amyloid- $\beta$ : Insights from Solid-State Nuclear Magnetic Resonance. *Cold Spring Harbor Perspect. Med.* **2016**, *6*, No. a024083.
- (63) Silverman, J.; Gibbs, E.; Rezaei, H.; Grznarova, K.; Guest, W.; Song, W.; Robin Hsiung, G.-Y.; Deslys, J.-P.; Roucou, X.; Wellington, C.; et al. An immunological epitope specific for toxic oligomeric  $A\beta$  in Alzheimer's disease. *Alzheimer's Dementia* **2012**, *8*, P625.
- (64) Silverman, J. M.; Gibbs, E.; Balducci, C.; Cowan, C.; Lamour, G.; Forloni, G.; Robin Hsiung, G.-Y.; Saward, L.; Wellington, C.; Cashman, N. R. An amyloid-beta oligomer epitope specific for toxic assemblages in Alzheimer's disease. *Alzheimer's Dementia* **2015**, *11*, P136–P137.
- (65) Zhou, R. Free energy landscape of protein folding in water: Explicit vs. implicit solvent. *Proteins: Struct., Funct., Bioinf.* **2003**, *53*, 148–161.
- (66) Maffucci, I.; Contini, A. An Updated Test of AMBER Force Fields and Implicit Solvent Models in Predicting the Secondary Structure of Helical,  $\beta$ -Hairpin, and Intrinsically Disordered Peptides. *J. Chem. Theory Comput.* **2016**, *12*, 714–727.
- (67) Tran, L.; Ha-Duong, T. Exploring the Alzheimer amyloid- $\beta$  peptide conformational ensemble: A review of molecular dynamics approaches. *Peptides* **2015**, *69*, 86–91.
- (68) Yang, M.; Teplow, D. B. Amyloid  $\beta$ -Protein Monomer Folding: Free-Energy Surfaces Reveal Alloform-Specific Differences. *J. Mol. Biol.* **2008**, *384*, 450–464.
- (69) Kleinjung, J.; Fraternali, F. Design and Application of implicit solvent models in biomolecular simulations. *Curr. Opin. Struct. Biol.* **2014**, *25*, 126–134 Theory and Simulation/Macromolecular Machines.
- (70) Chopra, G.; Summa, C. M.; Levitt, M. Solvent dramatically affects protein structure refinement. *Proc. Natl. Acad. Sci. U.S.A.* **2008**, *105*, 20239–20244.
- (71) Rokach, L.; Maimon, O. In *Data Mining and Knowledge Discovery Handbook*; Maimon, O., Rokach, L., Eds.; Springer, 2005; pp 321–352.
- (72) Case, D. A.; Babin, V.; Berryman, J.; Betz, R. M.; Cai, Q.; Cerutti, D. S.; Cheatham, T. E., III; Darden, T. A.; Duke, R.; Gohlke, H.; et al. *AMBER 14*; University of California: San Francisco, 2014.
- (73) Olsson, M. H. M.; Søndergaard, C. R.; Rostkowski, M.; Jensen, J. H. PROPKA3: Consistent Treatment of Internal and Surface Residues in Empirical pKa Predictions. *J. Chem. Theory Comput.* **2011**, *7*, 525–537.
- (74) Li, H.; Robertson, A. D.; Jensen, J. H. Very fast empirical prediction and rationalization of protein pKa values. *Proteins: Struct., Funct., Bioinf.* **2005**, *61*, 704–721.
- (75) Bas, D. C.; Rogers, D. M.; Jensen, J. H. Very fast prediction and rationalization of pKa values for protein-ligand complexes. *Proteins: Struct., Funct., Bioinf.* **2008**, *73*, 765–783.
- (76) Patriksson, A.; van der Spoel, D. A temperature predictor for parallel tempering simulations. *Phys. Chem. Chem. Phys.* **2008**, *10*, 2073–2077.
- (77) Case, D. A.; Darden, T. A.; Cheatham, T. E., I; Simmerling, C. L.; Wang, J.; Duke, R. E.; Luo, R.; Walker, R.; Zhang, W.; Merz, K. M.; et al. *AMBER 12*; University of California: San Francisco, 2012.
- (78) Hornak, V.; Abel, R.; Okur, A.; Strockbine, B.; Roitberg, A.; Simmerling, C. Comparison of multiple Amber force fields and development of improved protein backbone parameters. *Proteins: Struct., Funct., Bioinf.* **2006**, *65*, 712–725.
- (79) Maier, J. A.; Martinez, C.; Kasavajhala, K.; Wickstrom, L.; Hauser, K. E.; Simmerling, C. ff14SB: Improving the Accuracy of Protein Side Chain and Backbone Parameters from ff99SB. *J. Chem. Theory Comput.* **2015**, *11*, 3696–3713.
- (80) Onufriev, A.; Bashford, D.; Case, D. A. Exploring protein native states and large-scale conformational changes with a modified

generalized born model. *Proteins: Struct., Funct., Bioinf.* **2004**, *55*, 383–394.

(81) Ryckaert, J.-P.; Ciccotti, G.; Berendsen, H. J. Numerical integration of the Cartesian equations of motion of a system with constraints: molecular dynamics of n-alkanes. *J. Comput. Phys.* **1977**, *23*, 327–341.

(82) Neidigh, J. W.; Fesinmeyer, R. M.; Andersen, N. H. Designing a 20-residue protein. *Nat. Struct. Mol. Biol.* **2002**, *9*, 425–430.

(83) Rauscher, S.; Gapsys, V.; Gajda, M. J.; Zweckstetter, M.; de Groot, B. L.; Grubmüller, H. Structural Ensembles of Intrinsically Disordered Proteins Depend Strongly on Force Field: A Comparison to Experiment. *J. Chem. Theory Comput.* **2015**, *11*, 5513–5524.

(84) Vuister, G. W.; Bax, A. Quantitative J correlation: a new approach for measuring homonuclear three-bond  $J(\text{H}^N\text{H}^\alpha)$  coupling constants in  $^{15}\text{N}$ -enriched proteins. *J. Am. Chem. Soc.* **1993**, *115*, 7772–7777.

(85) Karplus, M. Vicinal Proton Coupling in Nuclear Magnetic Resonance. *J. Am. Chem. Soc.* **1963**, *85*, 2870–2871.

(86) Karplus, M. Contact Electron-Spin Coupling of Nuclear Magnetic Moments. *J. Chem. Phys.* **1959**, *30*, 11–15.

(87) Karplus, M.; Anderson, D. H. Valence-Bond Interpretation of Electron-Coupled Nuclear Spin Interactions; Application to Methane. *J. Chem. Phys.* **1959**, *30*, 6–10.

(88) Kabsch, W.; Sander, C. Dictionary of protein secondary structure: Pattern recognition of hydrogen-bonded and geometrical features. *Biopolymers* **1983**, *22*, 2577–2637.

(89) Chen, R.; Weng, Z. Docking unbound proteins using shape complementarity, desolvation, and electrostatics. *Proteins: Struct., Funct., Bioinf.* **2002**, *47*, 281–294.

(90) Mintseris, J.; Pierce, B.; Wiehe, K.; Anderson, R.; Chen, R.; Weng, Z. Integrating statistical pair potentials into protein complex prediction. *Proteins: Struct., Funct., Bioinf.* **2007**, *69*, 511–520.